Squall Line Dynamics: Analytical Formulation and Global Properties

Minghua Zhang
School of Marine and Atmospheric Sciences
Stony Brook University

Key Points:

1. Analytical formulation is presented to obtain stream functions of steady-state flows in squall lines along with far-side solutions
2. The formulation leads to prediction of the global properties of squall lines including propagation speed, cold pool depth, and mass fluxes
3. Squall lines are organized nonlinear dynamical systems with small degree of freedoms under given environmental wind and CAPE

Manuscript Submitted to *AGU Advances*

Corresponding address: minghua.zhang@stonybrook.edu

Abstract

Mesoscale convective systems (MCS) contribute about half of the world's precipitation and create flash flooding as well as other extreme weather events. Despite steady progress in research of these systems in the last several decades, theoretical understanding is still insufficient for them to be accurately parameterized in climate models and fully understood in numerical weather prediction models. This paper presents a theoretical formulation of one type of MCS, the steady-state squall lines. It describes the organization, propagation and cold pool properties of circulations within squall lines. Far-side analytical solutions are provided for selected special cases to illustrate the underlying physical processes of squall line flows. Numerical procedures are described for general conditions.

The formulation leads to the following prediction of the global properties of squall lines: Given the environmental profiles of wind and CAPE, the propagation speed, the depths and mass fluxes of the tilted ascending front-to-rear flow, the overturning circulation, and the descending rear inflow of the squall line, as well as the cold pool height and other global properties can be all determined from the cold pool intensity. The squall lines are therefore self-organized dynamical systems that have limited degree of freedoms in its global properties. Potential applications of theory are discussed.

Plain Language Summary

Mesoscale convective systems (MCS) contribute about half of the world's precipitation and create flash flooding as well as other extreme weather events. Their theoretical understanding is still limited. This paper presents a mathematical model of one type of MCS, the quasi-steady state two-dimensional squall lines. The model describes the organization, propagation and cold pool properties of squall lines.

The formulation leads to prediction of the global properties of squall lines: Given the environmental profiles of wind and Convective Available Potential Energy (CAPE), the propagation speed, the depths and mass fluxes of the tilted ascending front-to-rear flow, the overturning circulation, and the descending rear inflow of the squall line, as well as other properties can be all determined from the cold pool intensity. The squall lines are therefore self-organized dynamical systems that have limited degree of freedoms in its organizations. Results have the potential to improve prediction of squall lines and their parameterization in climate and weather prediction models.

1. Introduction

Mesoscale Convection Systems (MCS) are one of the most prominent weather systems that can be identified on satellite images of the Earth. They span spatial scales of tens to hundreds of kilometers and last several hours to days. They are shown by low brightness temperature in infrared satellite images because of their high top altitude, and by bright reflection in visible images because of their large loading of hydrometers. These systems account for about 50% of precipitation over the globe (e.g., Nesbitt et al., 2006; Houze, 2018; Feng et al., 2021a). They are estimated to contribute about 88% of latent heating above 7 kilometers over tropical land and 95% over tropical oceans (Liu et al., 2015). Most importantly, they create extreme precipitation events and associated weather that severely affect people's life.

Substantial progress has been made in the understanding of MCS in the last several decades as comprehensively reviewed by Houze (2004; 2018). These include insights from analysis of radar and satellite observations, field campaign data, and high-resolution numerical simulations. Numerical models are now able to simulate many salient features of MCS that includes the flow patterns, radar reflectivity and associated precipitations (e.g., Houze 2018; Prein et al., 2020; Stevens et al., 2020). Progress in theoretical understanding however is still limited owing to the highly nonlinear dynamics of MCS and its coupling with cloud and precipitation microphysics.

Much of the previous theoretical research on MCS has targeted squall lines that can be identified as quasi-linear precipitation systems on radar images. The quasi two-dimensional structure of squall lines offers some simplification for conceptualization of MCS organizations. Salient features of squall lines are summarized in the schematic Figure 1 that was adapted from Houze (2018). These include an ascending-front-to-rear flow (hereafter used interchangeably with the shorthand name "jump flow"), a descending-rear-inflow and returning flow (hereafter also referred to as "backside flow" or "cold-pool circulation"), the front-overturning-circulation (hereafter referred to as "overturning flow"), a cold pool, and a gust front at the head of the cold pool.

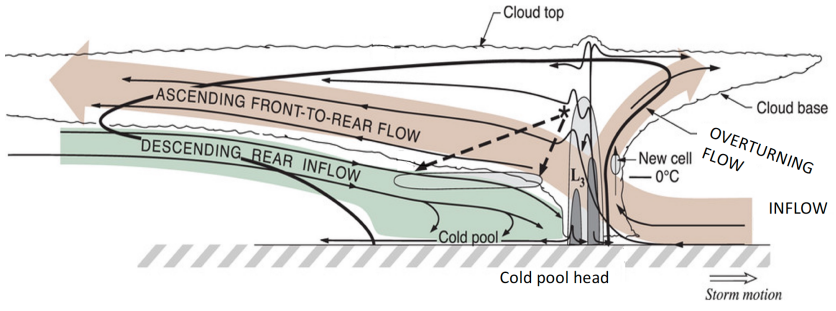

Figure 1. Conceptual model of the kinematic, microphysical, and radar echo structure of a squall line viewed in a vertical cross section oriented perpendicular to the convective line. Adapted from Figure 17.12 in Houze (2018).

The archetype model in Figure 1 is one type of flow configurations that has been abundantly confirmed in numerical simulations and observational analysis (e.g., Rotunno et al. 1988; Panda and Durran, 1996; Parker and Johnson, 2004; Alfaro and Khairoutdinov, 2015; Fan et al., 2017; Moncrieff et al., 2017; Houze 2018). Other possible configurations of flows will be discussed later in this paper.

While the archetype conceptualization of squall lines has formed an important theoretical framework to understand their organizations and relationship with environmental conditions, most past studies are limited to using specific combinations of the environmental wind, temperature, humidly along with various formulations of cloud and precipitation physics. The number of these combinations is endless. Studies have shown that the properties of squall lines are sensitive to the variation of these conditions, but the underlying physical mechanisms are not always clear. Better theoretical understanding is also necessary to establish the theoretical basis for improving the parameterization of these systems in climate models, which have suffered from many chronic biases attributed to convective schemes (e.g., Lin et al., 2017; Xie et al., 2019; Feng et al., 2021b; Christopoulos and Schneider; 2021). It is also important to improve their forecasts in numerical weather prediction models.

Among the few theoretical studies, the Rotunno–Klemp–Weisman (RKW) theory has enjoyed some success in predicting the optimal environmental condition of organized squall lines (Rotunno et al., 1988, hereafter referred to as RKW88 that also includes the following: Weisman et al., 1988; Weisman and Rotunno, 2004; Bryan and Rotunno, 2014). The theory states that the environmental condition of MCS is optimal when the vertical shear of the low-level environmental wind balances the circulation generated by a cold pool. The theory was derived semi-empirically based on analysis of the horizontal vorticity equation for two-dimensional squall lines and simulation results of numerical models. A parallel theory was presented in a sequence of papers by Moncrieff and collaborators about the steady-state of squall lines (Moncrieff and Green, 1972, hereafter referred to as MG72 that also includes the following: Moncrreff and Miller, 1976; Moncrieff, 1981; Thorpe et al. 1982; Moncrieff, 1992; Moncrieff, 2004). They emphasized the roles of both the Convective Available Potential Energy (CAPE) and available kinetic energy of the environment in the organization of squall lines. Based on constant wind shear and simplified CAPE that is linearly proportional to the vertical displacement of air parcels, they presented several archetypes of squall line systems and showed that these systems are controlled by a dimensionless Richardson number defined as the ratio of CAPE and the available kinetic energy.

The purpose of this paper is to advance the theoretical understanding of squall lines by building on top of these theoretical studies. We will present a mathematical model of the three interlocked flows in Figure 1: the ascending front-to-rear flow, the front overturning flow, and the descending rear-inflow on the backside. The far-side solution of these flows

allows for the prediction of the global properties of squall lines by using environment large-scale wind and CAPE. These include the propagation speed, cold pool height, the depths and mass fluxes of the three flows, and the pressure forces acting between them. The paper is organized as follows. Section 2 gives the controlling equations of the model, the setup of the mathematical problem and input environmental conditions. Sections 3 to 5 presents respectively the formulations of the ascending front-to-rear flow, the overturning circulation, and the descending-rear-flow and their far side solutions. Toy models are presented in each of these sections to gain insights about the physical processes governing the flow properties. Section 6 describes the interactions of the three flows and the global properties of squall lines. Section 7 discusses limitations of the theoretical analysis and potential applications of the theory. The last section contains a summary.

2. Controlling Equations and Environmental Conditions

2.1 The model

The controlling equations of squall lines used in this paper are similar to those used in many previous studies (e.g., Kleimp, 1987; RKW88; Pandya and Durran, 1996; Parker and Johnson, 2004). Written in the plane perpendicular to a squall line, the anelastic two-dimensional cloud model is as follows:

$$\frac{\partial u}{\partial t} + u\frac{\partial u}{\partial x} + w\frac{\partial u}{\partial z} = -\frac{1}{\bar{\rho}}\frac{\partial p}{\partial x} + F_u \tag{1}$$

$$\frac{\partial w}{\partial t} + u\frac{\partial w}{\partial x} + w\frac{\partial w}{\partial z} = -\frac{1}{\bar{\rho}}\frac{\partial p}{\partial z} + B + F_w \tag{2}$$

$$\frac{\partial \bar{\rho} u}{\partial x} + \frac{\partial \bar{\rho} w}{\partial z} = 0 \tag{3}$$

$$\frac{\partial}{\partial t}\left(\frac{\theta'}{\bar{\theta}}\right) + u\frac{\partial}{\partial x}\left(\frac{\theta'}{\bar{\theta}}\right) + w\frac{\partial}{\partial z}\left(\frac{\theta'}{\bar{\theta}}\right) = -w\frac{1}{\bar{\theta}}\frac{\partial \bar{\theta}}{\partial z} + \frac{1}{C_p \bar{T}}\dot{Q} \tag{4}$$

where u and w are the horizontal and vertical velocity, p is the perturbation air pressure relative to a reference vertical profile of the hydrostatic pressure in the environment; $\bar{\rho}$ is the density of the environmental air, assumed to be a function of height only; B is the buoyancy force; θ' and $\bar{\theta}$ are respectively the perturbation and environmental potential temperatures; F_u, F_w denote molecular and turbulent mixing of momentum; $\dot{Q}$ is the diabatic and other sources of heating. The Coriolis force is neglected in this paper. It can be incorporated if necessary for very long lived systems. The mass continuity equation (3) constrains the perturbation pressure as:

$$\nabla^2 p = -\bar{\rho}\left[\left(\frac{\partial u}{\partial x}\right)^2 + \left(\frac{\partial w}{\partial z}\right)^2 + 2\frac{\partial u}{\partial z}\frac{\partial w}{\partial x} - w^2\frac{\partial^2 ln\bar{\rho}}{\partial z^2}\right] + \left(\frac{\partial \bar{\rho} B}{\partial z} + \frac{\partial \bar{\rho} F_u}{\partial x} + \frac{\partial \bar{\rho} F_w}{\partial z}\right) \tag{5}$$

The buoyancy force in the vertical momentum equation (2) is

$$B = \frac{\rho'}{\bar{\rho}}g + B' \approx \frac{\theta'}{\bar{\theta}}g + B' \tag{6}$$

where ρ' is the density deviation from the reference profile; B' is the buoyance component due to loading of hydrometers. In the following, since the density perturbation is no longer used, we will simply use ρ to denote $\bar{\rho}$.

The thermodynamic equation (4) can be written in the form of the buoyancy as defined in (6):

$$\frac{\partial B}{\partial t} + u\frac{\partial B}{\partial x} + w\frac{\partial B}{\partial z} = -wN_d^2 + \frac{g}{C_p\bar{T}}\dot{Q} + \frac{DB'}{Dt} \tag{7}$$

$$N_d^2 = \frac{g}{\bar{\theta}}\frac{\partial \bar{\theta}}{\partial z} \tag{8}$$

N_d is the Brunt-Väisälä frequency of the dry atmosphere. We introduce a generalized frequency N for the purpose of the present study:

$$N^2 = N_d^2 - \frac{1}{w}\left(\frac{g}{C_p\bar{T}}\dot{Q} + \frac{DB'}{Dt}\right) \tag{9}$$

N^2 contains the impact of diabatic heating and loading of hydrometers. $N^2 = 0$ corresponds to a neutral atmosphere. Condensation and evaporation may take place when air moves up or down along moist adiabats. $N^2 < 0$ corresponds to an unstable atmosphere. Using (9), we write (7) in the following simplified form:

$$\frac{\partial B}{\partial t} + u\frac{\partial B}{\partial x} + w\frac{\partial B}{\partial z} = -wN^2 \tag{10}$$

This leads to an equation of the buoyancy conservation as

$$\frac{DB}{Dt} = -N^2\frac{Dz}{Dt} \tag{11}$$

where $\frac{D}{Dt}$ is the total derivative following an air parcel.

As in MG72 and RKW88, the equations of motion (1) and (2) are combined to form the vorticity equation:

$$\frac{D}{Dt}\left(\frac{\eta}{\rho}\right) = -\frac{1}{\rho}\frac{\partial B}{\partial x} + \frac{1}{\rho}F_\eta \tag{12}$$

where η is the horizontal vorticity along the y axis:

$$\eta = \frac{\partial u}{\partial z} - \frac{\partial w}{\partial x} \tag{13}$$

and F_η represents the effect of dissipative forces on the vorticity. (12) is not exactly the same as (1)-(3). The derivation involves an approximation that the change of the horizontal pressure gradient force with height, whenever it is important in the vorticity budget, is dominated by the change associated with the pressure field rather than by the change of the mean density of the atmosphere. This should be an acceptable approximation based on available numerical simulation results that use (1)-(5) directly for squall lines. To make the set of equations in this paper self-contained, I have included the derivations and approximations of (5) and (12) in Appendix A.

An energy conservation equation can be derived after multiplying (1) and (2) by the respective velocity components as follows:

$$\frac{D}{Dt}\left(\frac{V^2}{2}+\frac{p}{\rho}\right)-B\frac{Dz}{Dt}=F_E \tag{14}$$

where F_E is the dissipative sources or sinks of kinetic energy. This is the Bernoulli form of energy conservation. (14) is also not exactly the same as (1)-(3). A small term associated with the work performed by the perturbation pressure of an expanding or contracting air parcel is neglected. Because the perturbation pressure is typically orders of magnitude smaller that the hydrostatic pressure of the environment, this should be an acceptable approximation. I have also included the derivation and approximation of (14) in Appendix A.

Our interest is in the nonlinear laminar flows. The dissipative terms are assumed to play minor roles and will be neglected, which is an obvious oversimplification but necessary to make the problem tractable. As in MG72, if we integrate the buoyancy equation, the vorticity equation and the energy equation with time for an air parcel moving from an initial initial time t_0 at altitude z_0 to a later time t, we can obtain the following conservation equations:

$$B|_{t,z} = B|_{t_0,z_0} - \int_{z_0}^{z} N^2 dz \tag{15}$$

$$\left(\frac{\eta}{\rho}\right)\Big|_{t,z} = \left(\frac{\eta}{\rho}\right)\Big|_{t_0,z_0} - \int_{t_0}^{t} \frac{1}{\rho}\frac{\partial B}{\partial x} dt \tag{16}$$

$$\left(\frac{V^2}{2}+\frac{p}{\rho}\right)\Big|_{t,z} = \left(\frac{V^2}{2}+\frac{p}{\rho}\right)\Big|_{t_0,z_0} + \int_{z_0}^{z} B(z_0,z)\mathrm{dz} \tag{17}$$

where all integrals are along the air parcel trajectories. (16) states that vorticity is conserved along an air parcel trajectory subject to change of the accumulated forcing by the horizontal gradient of the buoyancy, while (17) states that the energy is conserved along the parcel trajectory subject to change by the work of the buoyancy. Because of the relationship between kinetic energy and pressure in (17), in later discussions we also refer the kinetic energy as dynamic pressure, a terminology that is commonly used in hydrodynamics.

The mass continuity equation (3) allows the two velocity components to be expressed by the stream function as:

$$\rho u = \frac{\partial \psi}{\partial z} \tag{18}$$

$$\rho w = -\frac{\partial \psi}{\partial x} \tag{19}$$

The vorticity in (13) is then expressed in terms of the stream function as:

$$\eta = \frac{1}{\rho}\left(\frac{\partial^2 \psi}{\partial x^2}+\frac{\partial^2 \psi}{\partial z^2}+\frac{1}{H_s}\frac{\partial \psi}{\partial z}\right) \tag{20}$$

where H_s is the scale height:

$$H_s = -\frac{1}{\rho}\frac{\partial \rho}{\partial z} \tag{21}$$

Here the symbol H_s is used instead of the customary H, because the latter will be used to denote the height of the model domain.

For steady state motions, the trajectories of air parcels are the same as streamlines. Following MG72, we can write the buoyancy forcing of the vorticity in the following format by the using the chain rule of derivatives and (19) in (16):

$$\begin{aligned}\left(\frac{\eta}{\rho}\right)\Big|_{t,z} &= \left(\frac{\eta}{\rho}\right)\Big|_{t_0,z_0} - \int_{t_0}^{t} \frac{1}{\rho}\frac{\partial B(\psi,z)}{\partial \psi}\,\frac{\partial \psi}{\partial x}\,dt = \left(\frac{\eta}{\rho}\right)\Big|_{t_0,z_0} + \int_{t_0}^{t} \frac{\partial B(\psi,z)}{\partial \psi} w\,dt \\ &= \left(\frac{\eta}{\rho}\right)\Big|_{t_0,z_0} + \int_{z_0}^{z} \frac{\partial B(\psi,z)}{\partial \psi}\,dz = \left(\frac{\eta}{\rho}\right)\Big|_{t_0,z_0} + \int_{z_0}^{z} \frac{\partial B(z_0,z)}{\partial z_0}\frac{\partial z_0}{\partial \psi}\,dz \\ &= \left(\frac{\eta}{\rho}\right)\Big|_{t_0,z_0} + \int_{z_0}^{z} \frac{\partial B(z_0,z)}{\partial z_0}\frac{1}{\rho_0 u_0}\,dz\end{aligned} \tag{22}$$

To our knowledge, MG72 was the first to express the vorticity forcing as in the second term on the right-hand side of (22). The importance of this MG72 form is that the accumulated vorticity sources along a streamline can be expressed as the buoyance difference of the parcels originating from neighboring altitudes that is independent of the specific shape of the trajectories.

Here and in the following sections, steady state is assumed to be in the reference frame propagating with the squall. It can be shown that under steady-state condition, the vorticity equation (22) is identical to the momentum equation in the natural coordinate system of a streamline in the direction perpendicular to it, subject to minor approximation stated earlier for the vorticity equation. The proof is provided in Appendix B. The Bernoulli equation is the same as the momentum equation along the streamlines. These equations are written here since they are useful to interpret the relationship between pressure field and the shape of the streamlines:

$$\frac{V^2}{R} = \left(-\frac{\nabla p}{\rho} + B\vec{k}\right)\cdot \vec{n} = F_n \tag{23}$$

$$\frac{\partial}{\partial s}\left(\frac{V^2}{2}\right) = \left(-\frac{\nabla p}{\rho} + B\vec{k}\right)\cdot \vec{s} = F_s \tag{24}$$

where R is the curvature radius of a streamline; $V^2 = u^2 + w^2$; $\vec{k}$ is a unit vector in the z direction. $\vec{n}$ and $\vec{s}$ are unit vectors perpendicular and parallel to the streamline as shown in Figure 2; F_n and F_s are the projection of pressure gradient and buoyancy forces in the $\vec{n}$ and $\vec{s}$ directions.

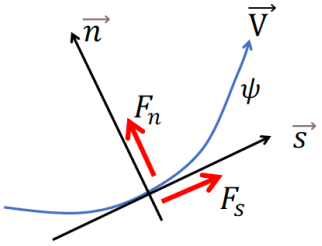

Figure 2. Streamline (ψ) and the natural coordinate system with tangential and perpendicular forces F_s and F_n to accelerate the flow or bend the streamline.

(23) states that for a streamline to bend or turn direction, i.e., with finite values of the curvature radius R, normal force is necessary. Since buoyancy force is pointed vertically, the force from the dynamic pressure field plays a major role in steering the flow horizontally and in determining

the shape of the stream lines. (24) states the obvious fact that acceleration and deceleration along the streamlines are carried out by the combined projection of the pressure gradient force and the buoyancy force in the direction of the streamlines. If the forces of F_n and F_s are known, (24) can be integrated to obtain the wind speed, while (23) can be used to derive the curvature. The streamlines can then be determined as long as the initial conditions of a parcel are known. The procedure is described in Appendix B. These forces however are part of the unknown solutions, since the pressure field is interactive with the flow field as in (5).

2.2 Setup of the Mathematical Problem

Using (20), we can write the vorticity equation (22) as the following:

$$\frac{\partial^2\psi}{\partial x^2}+\frac{\partial^2\psi}{\partial z^2}+\frac{1}{H_s}\frac{\partial\psi}{\partial z}=\frac{\rho^2}{\rho_0}\eta_0+\frac{\rho^2}{\rho_0 u_0}\int_{z_0}^{z}\frac{\partial B(z_0,z)}{\partial z_0}\,dz \tag{25}$$

in which subscript "0" represents the initial conditions. We seek solution of the stream function $\psi(x,z)$ in a domain $x\,\epsilon\,[-L,L]$ and $z\,\epsilon\,[0,H]$ where L is sufficiently large so that at $x=\pm L$ the motion can be assumed to be horizontal. H is the top of the model where a rigid boundary is assumed, typically at the level of the tropopause. The model top can be actually formulated as a free boundary with a modulating height of $z_H=H(x)$, but then additional equations are needed to describe the stratosphere. This is not considered in the present paper. Without loss of generality, we assume that the separation point between the ascending flow and the descending backside flow at the surface is the origin $(x,z)=(0,0)$, as schematically shown in Figure 3. Since in the two-dimensional framework, the streamlines do not cross, they can be used as free boundaries of different flow regimes subject to continuity requirements across the boundaries.

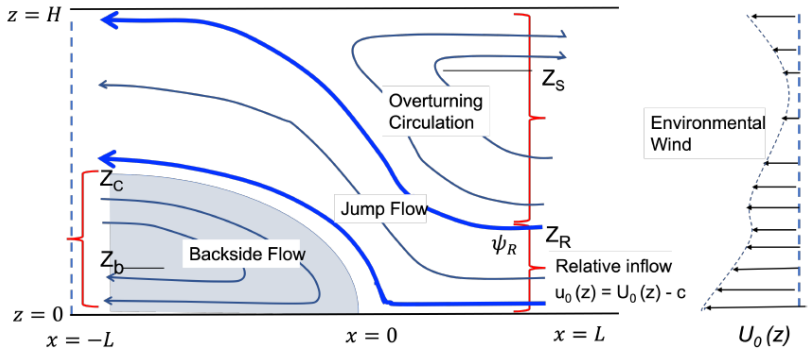

Figure 3. Schematics of the solution domains and streamlines of the jump flow, the overturning circulation, and the backside flow. The blue streamlines separate the three flows. z_R is the altitude of the inflow separating the jump flow and the overturning circulation. z_S is the altitude separating the inflow and outflow in the overturning circulation. z_c is the altitude separating the jump flow and the backside flow on the far left. z_b is the altitude separating the inflow and outflow in the cold pool. The environmental wind profile is $U_0(z)$; the relative inflow is $u_0(z)=U_0(z)-c$, where c is the propagation speed of the squall line.

The three regions of the jump flow, the overturning circulation and backside flow are separated by a streamline dividing the ascending and descending motions, and a streamline dividing the ascending front-to-rear flow and the overturing circulation highlighted in Figure 3. Depending on the environmental conditions, steady-state solutions may not exist, or the solution may only contain two regions without the overturning circulation, or the jump flow, or the backside circulation. Figure 3 is one configuration of possible solutions. Other flow types may exist under suitable conditions of wind and CAPE. These include the addition of a counterclockwise circulation on the back side immediately below the jump flow that is sandwiched between the jump flow and backside flow below in the figure; intrusion of the descending cold pool flow into the front of the storm, and elevated jump flow with near-surface air in the inflow passing through the cold pool. The model can be generalized to include these flow patterns. However, to limit the length of the paper, the governing equation and the boundary conditions of the stream functions in the three regions schematically in the typical conceptual model outlined in Figure 3 will be formulated in this paper.

Once the stream function is known, the pressure field can be derived from the Bernoulli equation (17) as

$$p = -\frac{1}{2\rho}|\nabla\psi|^2 + \rho\left[\int_{z_0}^{z} B(z_0, z)\mathrm{dz} + \left(\frac{1}{2}V_0^2 + \frac{p_0}{\rho_0}\right)\right] \tag{26}$$

2.3 Environmental Conditions

The diabatic heating $\dot{Q}$ in (9) includes latent heating from condensation of water vapor and freezing of liquid, cooling from evaporation and melting of hydrometers, as well as radiative and dissipative heating. The heating of reversible ascending and descending air with phase changes between the water vapor and liquid water are typically expressed as

$$\dot{Q} \approx L_v \frac{dq_l}{\partial t} + \dot{Q}_r = L_v \frac{dq_l}{dz} w + \dot{Q}_r \tag{27}$$

where q_l is the liquid mixing ratio, L_v is the latent heating of condensation. Here only the liquid phase is used, but this can be generalized to include ice. $\dot{Q}_r$ is the radiative and dissipative sources. The generalized moist frequency N in (9) then measures the vertical stability of the atmosphere after consideration of heating and loading of hydrometers:

$$N^2 = N_d^2 - \frac{g}{C_p\bar{T}}\frac{\dot{Q}}{w} - \frac{1}{w}\frac{DB'}{Dt} \approx \left(\frac{g}{\bar{\theta}}\frac{\partial\bar{\theta}}{\partial z} - \frac{L_v g}{C_p\bar{T}}\frac{dq_l}{dz} - \frac{g}{C_p\bar{T}}\frac{\dot{Q}_r}{w} - \frac{1}{w}\frac{DB'}{Dt}\right) \tag{28}$$

An important assumption to be made is that N^2 is known and it depends only on the initial and final altitudes of an air parcel under given environmental conditions, i.e., $N^2 = N^2(z_0, z)$. This is what is typically used in parcel models.

N^2 can take different values in different flow regions in Figure 3. With a known N^2, the buoyancy equation (15) leads to the following:

$$B(z_0, z) = B(z_0, z_0) - \int_{z_0}^{z} N^2(z_0, z)dz \tag{29}$$

$B(z_0, z)$ denotes the buoyancy of an air parcel moving from altitude z_0 to z. $CAPE$, the work that the environment does to a unit mass of air when it moves from altitude z_0 to z is

$$CAPE(z_0, z) = \int_{z_0}^{z} B(z_0, z)dz \tag{30}$$

If $CAPE(z_0, z)$ is known, the buoyancy can be obtained as:

$$B(z_0, z) = B(z_0, z_0) + \frac{\partial CAPE(z_0,z)}{\partial z} \tag{31}$$

$CAPE(z_0, z)$ or buoyancy $B(z_0, z)$ is assumed to be available from the environmental vertical profiles of atmospheric temperature and humidity. They are to be calculated for all altitudes of z_0 and z, including cases of $z_0 > z$ for descending motions. $CAPE(z_0, z)$ is positive in an unstable atmosphere when air originating from lower levels (small z_0) passes the lifting condensation level (LCL) and the level of free convection (LFL) to reach sufficient height to overcome the convective inhibition (CIN). Positive $CAPE(z_0, z)$ is also possible for descending air that contains sufficient sources of condensate to evaporate.

Besides $B(z_0, z)$ and $CAPE(z_0, z)$, another environmental variable $G(z_0, z)$ is introduced for the model as the following:

$$G(z_0, z) = \int_{z_0}^{z} \frac{\partial B(z_0,z)}{\partial z_0}\, dz = -\frac{\partial}{\partial z_0}\int_{z_0}^{z} B(z_0, z)\, dz = -\frac{\partial CAPE(z_0,z)}{\partial z_0} \tag{32}$$

G measures the difference of CAPE between air parcels originating from different altitudes when they reach the same altitude. The contrast of (32) from the buoyance force (31) should be noted. In the case of zero initial buoyancy and reversable thermodynamic process, $G(z_0, z)$ is equal to the transpose of $B(z, z_0)$, i.e.,

$$G(z_0, z) = B(z, z_0) \tag{33}$$

This is because

$$CAPE(z_0, z) = -CAPE(z, z_0) \tag{34}$$

which states that the energy required for a parcel to rise from z_0 to z has the same magnitude as that of the parcel descending from z to z_0 but with an opposite sign.

Since the steady state assumption is relative to the propagating squall line, the wind fields in the conservation equations of (15)-(17) and (25) are all relative to the propagation speed of the squall line. The environmental wind will be denoted as $U(z)$. The storm relative environmental flow is then

$$u_0(z) = U(z) - c \tag{35}$$

where c is the propagation speed of the system, an unknown variable. c will be part of the model solution.

With these definitions, the vorticity and energy equations of (25) and (17) can be written as the followings:

$$\frac{\partial^2 \psi}{\partial x^2} + \frac{\partial^2 \psi}{\partial z^2} + \frac{1}{H_s}\frac{\partial \psi}{\partial z} = \frac{\rho^2}{\rho_0(z_0)}\left[\eta_0(z_0) + \frac{1}{u_0(z_0)}G(z_0, z)\right] \tag{36}$$

$$\left(\frac{V^2}{2}+\frac{p}{\rho}\right)\Big|_{t,z} = \left(\frac{V^2}{2}+\frac{p}{\rho}\right)\Big|_{t_0,z_0} + CAPE(z_0,z) \tag{37}$$

The subject of this paper is to determine ψ, along with the unknown propagation speed c, under given environmental wind profile of $U(z)$ and $CAPE(z_0,z)$, to which $B(z_0,z)$ and $G(z_0,z)$ are related by (31) and (32). Lifting is not separately considered. It is internally provided by either the buoyancy force or the pressure gradient force.

3 The Ascending Front-To-Rear Flow

3.1 Formulation

We denote the altitude of the boundary separating the jump flow and the overturning circulation on the far right of Figure 3 as z_R, and the altitude of the boundary separating the jump flow and the backside flow on the far left as z_c, both of which are marked in the figure. The streamline originating at $z_0 = z_R$ in the inflow on the far right reaches the model top of height H on the downstream side on the far left, with value of the stream function as ψ_R. The streamline originating at $z_0 = 0$ in the inflow reaches $z = z_c$ on the far left, with the value of the stream function as 0 without loss of generality. These two streamlines separate the three flow regions. The altitudes of z_R, z_c and the value of ψ_R as well as the propagation speed c will be ultimately determined by the model. They are temporarily assumed to be known. The inflow below the altitude z_R is referred to as the lower inflow to be distinguished from the upper inflow of the overturning circulation above it.

With the above definitions, at the inflow boundary of $x = L$ and $z_0 \in [0, z_R]$, the storm relative inflow, the stream function, and the horizontal vorticity are as follows:

$$u_0(z_0) = U(z_0) - c, \quad \frac{\partial \psi}{\partial z_0} = \rho u_0(z_0), \text{ and } \eta_0 = \frac{\partial u_0}{\partial z_0} = \eta_0(z_0) \tag{38}$$

ψ and η_0 as a function of z_0 are uniquely determined by the vertical profiles of the environmental density and wind with a given the propagation speed c. The assumption of the flow regime in Figure 3 means that ψ is a monotonic function of z_0 in the region of the jump flow, hence from $\psi = \psi(z_0)$, we can get the inversion of z_0 as a function of ψ:

$$z_0 = z_0(\psi) \tag{39}$$

With substitution of (39) into the vorticity equation (36) and using (38), the stream function of the jump flow is governed by the following equation:

$$\frac{\partial^2 \psi}{\partial x^2} + \frac{\partial^2 \psi}{\partial z^2} + \frac{1}{H_s}\frac{\partial \psi}{\partial z} = F(\psi, z) \tag{40}$$

$F(\psi, \mathrm{z})$ on the right hand of (36) is

$$F(\psi, \mathrm{z}) = \frac{\rho^2(z)}{\rho[z_0(\psi)]}\{\eta_0[z_0(\psi)] + \frac{1}{u_0[z_0(\psi)]} G[z_0(\psi), \mathrm{z}]\} \tag{41}$$

where all the brackets and parenthesis denote a functional relationship. $F(\psi, \mathrm{z})$ is calculated from the environmental fields of the inflow u_0 and G. (40) and (41) are a nonlinear elliptic equation governing $\psi = \psi(x, z)$. $F(\psi, \mathrm{z})$ in (41) could be a highly nonlinear function of ψ depending on the environmental inflow $U(z_0)$ and $CAPE(z_0, z)$. But it is not as onerous as it looks in numerical calculations, and it can be analytically expressed under some special cases as will be discussed later.

For numerical calculation, iteration is often used to solve elliptic equations. After an initial guess of $\psi^*(x, z)$ at a set of grids in the domain written as $\psi^*_{i,j}$ with (i, j) as (x, z) indices of a grid, a unique origination altitude z_0^* can be obtained by using the mapping relation (39) for each $\psi^*_{i,j}$. Since $\psi^*_{i,j}$ must lie in the range of 0 to ψ_R, z_0^* will lie in the range of 0 to z_R. A second round of interpolations using z_0^* as input and (38) and (32) gives the values of $\eta_0(z_0^*)$, $u_0(z_0^*)$, $\rho_0(z_0^*)$, $G(z_0^*, \mathrm{z})$. These completely determine the value of $F^*_{i,j}\left(\psi^*_{i,j}, \mathrm{z}\right)$ in (41) that corresponds to the initial guess of the stream function $\psi^*_{i,j}$. Standard numerical algorithms can then be applied to obtain the solution of (40) if the boundary conditions of the stream function ψ in the irregularly shaped flow region sandwiched between the two blue streamlines in Figure 3 are known.

3.2 Boundary Conditions

On the side of the inflow $x = L$:

$$\psi(x = L, z) = \int_0^z \rho u_0(z_0)\, dz_0 \quad \text{for} \quad z \in [0, z_R] \tag{42}$$

From (42), the value of the stream function at the upper boundary is determined as

$$\psi_R = \int_0^{z_R} \rho u_0(z_0)\, dz_0 \tag{43}$$

On the side of the outflow $x = -L, z \in [z_c, H]$. (40) is a one-dimensional 2nd order differential equation

$$\frac{d^2\psi}{dz^2} + \frac{1}{H_s}\frac{d\psi}{dz} = F(\psi, z) \tag{44}$$

with known boundary conditions of

$$\psi(z = z_c) = 0 \tag{45}$$

$$\psi(z = H) = \psi_R \tag{46}$$

(44) can be solved numerically by using the same method as described at the end of the previous subsection. This far-side solution of $\psi_{-L}(z)$ forms the second boundary condition of $\psi(x, y)$:

$$\psi(x = -L, z) = \psi_{-L}(z) \quad \text{for} \quad z \in [z_c, H] \tag{47}$$

The top and lower boundary conditions of $\psi(x, y)$ are at $z = h_0(x), z = h_R(x)$:

$$\psi|_{z=h_0(x)} = 0 \tag{48}$$

$$\psi|_{z=h_R(x)} = \psi_R \tag{49}$$

where $h_0(x)$ and $h_R(x)$ are two free boundaries that separate the three regions of the flow in Figure 3. $h_0(x)$ and $h_R(x)$ are to be determined based on the continuity of pressure across the

boundaries. If the solutions in the other two regions are known and their pressure fields at the boundaries are assumed to be $p_0(x)$ and $p_R(x)$ respectively, then based on the Bernoulli equation (37),

$$-\frac{1}{2\rho}|\nabla\psi|^2 + \rho\left[\text{CAPE}(0,z) + \frac{1}{2}u_0^2(0)\right] = p_0(x) \text{ at } z = h_0(x) \tag{50}$$

$$-\frac{1}{2\rho}|\nabla\psi|^2 + \rho\left[\text{CAPE}(z,H) + \frac{1}{2}u_0^2(z_R)\right] = p_R(x) \text{ at } z = h_R(x) \tag{51}$$

The pressure perturbation in the inflow $x = L$ has been assumed as zero in (50)-(51) where the reference pressure is defined. $h_0(x)$ and $h_R(x)$ themselves satisfy the following boundary conditions:

$$h_0(x) = \begin{cases} 0 & for\ x = 0 \\ z_c & for\ x = -L \end{cases} \tag{52}$$

$$h_R(x) = \begin{cases} z_R & for\ x = L \\ H & for\ x = -L \end{cases} \tag{53}$$

Given the pressure field $p_0(x)$ and $p_R(x)$ at the interfaces of the regions from the outer solutions, Equations (40) and (41) and boundary conditions of (42), (47), (48)-(53) completely determine the solution of the jump flow and the shape functions $h_0(x)$ and $h_R(x)$ of the two streamlines at the upper and lower boundaries. The outer solutions will be formulated in Section 4 and Section 5 respectively.

3.3 Momentum Constraint on the Jump Flow

The steady-state momentum equation of u without dissipation in (1) can be written as

$$\nabla \cdot (\rho\,\vec{V}u) = -\frac{\partial p}{\partial x} \tag{54}$$

Integrating the above equation over the whole region of the jump flow Ω_a and using the Gauss's theorem on the divergence term, we get

$$\oint_{\partial\Omega_a}\left(\rho u\vec{V}\cdot\vec{n}\right)ds + \iint_{x,z\epsilon\,\Omega_a}\frac{\partial p}{\partial x}dxdz = 0 \tag{55}$$

Considering that the normal velocity to the streamlines is zero, we can obtain

$$\int_{z_c}^{H}\rho u^2(x=-L)dz + \int_{z_C}^{H}p(x=-L,z)dz = \int_0^{z_R}\rho u_0^2 dz_0 + (P_{\psi=\psi_R} - P_{\psi=0}) \tag{56}$$

where we have assumed the perturbation pressure at $x = L$ in the inflow to be zero. $P_{\psi=0}$ and $P_{\psi=\psi_R}$ are the integrated pressure along the streamlines of $\psi = 0$ and $\psi = \psi_R$ defined as the following:

$$P_{\psi=0} = \int_0^{z_c} p(x_{\psi=0}, z)dz \tag{57}$$

$$P_{\psi=\psi_R} = \int_{z_R}^{H} p(x_{\psi=\psi_R}, z)\,dz \tag{58}$$

$x_{\psi=0}$ and $x_{\psi=\psi_R}$ are functions of z that can be expressed as the inverse functions of the two free boundaries $z = h_0(x)$, and $z = h_R(x)$:

$$x_{\psi=0} = h_0^{-1}(z),\ and\ \ x_{\psi=\psi_R} = h_R^{-1}(z). \tag{59}$$

The physical meaning of (56) is straightforward: The momentum flux out of the left boundary is equal to the momentum flux in the inflow plus the difference of pressure at the right and left boundaries. The total pressure at the right boundary is the horizontal pressure force acting on the jump flow by the overturning circulation; the total pressure at the left boundary consists of the total force acting by the backside flow on the jump flow and the pressure in the outflow.

3.4 Far-Side Solution: A Toy Model

As an illustration, we use the simplest model of a neutral atmosphere without shear of the mean wind. Obviously, there would be no squall lines. But the model can describe gravity currents, from which some important insights can be obtained. There is a wealth of literature on gravity currents, including models with shear (e.g., Benjamin 1968; Xu, 1992; Xue, 1997; Byran and Rotunno, 2014). In the following description of the toy model, whenever feasible, I will add how wind shear, CAPE, and flow regimes might impact results of the gravity current. We also assume ρ to be constant so that the term involving H_s in the vorticity can be dropped.

3.4.1 The solution

In this toy model, according to (38), $u_0 = U - c,\ \eta_0 = 0$. Following their definitions, $B = G = F = 0$. Thus, based on (40)-(41), the stream function in the whole jump flow is governed by the following simple equation with zero vorticity everywhere including in the near field:

$$\frac{\partial^2 \psi}{\partial x^2} + \frac{\partial^2 \psi}{\partial z^2} + \frac{1}{H_s}\frac{\partial \psi}{\partial z} = 0 \tag{60}$$

At $x = L$, the inflow boundary condition (42) gives

$$\psi = \rho u_0 z, \text{ and } \psi_R = \rho u_0 z_R \tag{61}$$

The far-side solution of (60) at $x = -L$ is

$$\psi = \rho u_h (z - z_c) \tag{62}$$

which satisfies the boundary condition of $\psi = 0$ at $z = z_c$ in (48). u_h is determined by the boundary condition (49) $\psi(H) = \psi_R = \rho u_0 z_R$, and so

$$\rho u_h (H - h) = \rho u_0 z_R \tag{63}$$

Thus,

$$u_h = \frac{z_R}{H - z_c} u_0 \tag{64}$$

u_h is the horizontal velocity at the left boundary, which is constant since the vorticity is zero and there is no shear. (64) is simply a form of the mass continuity equation, with the inflow mass flux at $x = L$ in a layer of depth z_R equal to an outflow mass flux at $x = -L$ of depth $H - z_c$. If the depth of the inflow layer is larger than the thickness of the outflow layer $z_R > H - z_c$, then $|u_h| > |u_0|$. This is the case of typical study on gravity currents in which the inflow depth z_R is often assumed to be equal to the whole depth of the fluid. If $z_R < H - z_c$, in which a layer of relatively thin inflow exits with a larger depth at the left boundary, the outflow speed is then smaller than the speed of the inflow $|u_h| < |u_0|$.

3.4.2 Propagation Speed

The near-field solution cannot be determined without knowing the solutions in outer regions. A special case of the backside solution is a motionless cold pool relative to the propagating storm. We assume a constant negative buoyancy $B = -b$ on the backside in the cold pool, where b is its intensity. According to (30), $CAPE(z_0, z)$ in the cold pool is simply $b(z_0 - z)$. The Bernoulii equation (17) becomes a hydrostatic balance in the cold pool that gives the difference of pressure in the cold pool with the pressure at the interface $z = h_0(x)$ as:

$$p(x,z) - p_{h_0(x)} = \rho b[h_0(x) - z] \tag{65}$$

At the surface,

$$p(x,0) - p_{h_0(x)} = \rho b h_0(x) \tag{66}$$

At the far-side $x = -L$ on the left, the pressure difference between the surface and the interface at $h_0 = z_c$ is

$$p(-L,0) - p_{z_c} = \rho b z_c \tag{67}$$

If z_c is known, through some tedious derivations, the propagation speed of cold pool can be inferred. The bottom line is that the dynamic pressure of the inflow needs to be balanced by the pressure from the backside in the propagating reference frame, and this constrains the relative speed of the inflow at the surface, thus the propagation speed of the squall line. For the sake of completeness, the formal derivation is given below.

Using the Bernoulli equation in the motionless cold pool from $(x,z) = (-L,0)$ to $(x,z) = (0,0)$ gives

$$p(0,0) = p(-L,0) \tag{68}$$

where the origin (0,0) is the head location of the cold pool. From (67) and (68), we can relate the head pressure $p(0,0)$ and the pressure at the top of the cold pool p_{z_c} as

$$p(0,0) = p_{z_c} + \rho b z_c \tag{69}$$

Using the Bernoulli equation a second time for $\psi = 0$ in the jump flow between $(x,z) = (L,0)$ to $(0,0)$ gives the dynamic pressure at the head of the cold pool as in the following, since in the jump flow the relative velocity is zero at the cold pool head and perturbation pressure is zero at $(L,0)$:

$$p(0,0) = \frac{1}{2}\rho u_0^2 \tag{70}$$

The pressure at the cold pool head in the jump flow is same as that in the cold pool because of continuity requirement of the pressure field. Eliminating $p(0,0)$ in (69) and (70) gives the following relationship between the p_{z_c}, the inflow velocity and the cold pool height z_c:

$$p_{z_c} = \tfrac{1}{2}\rho u_0^2 - \rho b z_c \tag{71}$$

Using the Bernoulli equation a third time for $\psi = 0$ from $(x,z) = (0,0)$ to $(x,z) = (-L,z_c)$ in the jump flow gives another relationship to obtain p_{z_c}:

$$\frac{p_{z_c}}{\rho} = \frac{p(0,0)}{\rho} - \frac{1}{2}u_h^2 \tag{72}$$

Substituting $p(0,0)$ in (70) into (72), we have

$$p_{z_c} + \frac{1}{2}\rho u_h^2 = \frac{1}{2}\rho u_0^2 \tag{73}$$

While the derivation process of (71) and (73) is cumbersome, their physical meanings are straightforward: (72) states that the pressure deficit p_{z_c} at $z = z_c$ relative to the dynamic head pressure $(\frac{1}{2}\rho u_0^2)$ equals to the reduction of the hydrostatic pressure in the cold pool. Equation (73) states that the sum of the pressure at p_{z_c} and the dynamic pressure $\frac{1}{2}\rho u_h^2$ at $z = z_c$ is equal to the head dynamic pressure $\frac{1}{2}\rho u_0^2$.

Eliminating p_{z_c} from (72) and (73) also eliminates $\frac{1}{2}\rho u_0^2$, which leads to the following:

$$\frac{1}{2}u_h^2 = bz_c \tag{74}$$

Replacing u_h by the velocity of the exit flow from the previously obtained solution (64), we can get

$$\left(\frac{z_R}{H-z_c}u_0\right)^2 = 2bz_c \tag{75}$$

$$u_0^2 = 2bz_c\frac{(H-z_c)^2}{z_R^2} \tag{76}$$

Since $u_0 = U - c$ where U is the environmental wind relative to an observer on the ground, the above equation constrains the propagation speed of the cold pool when the depth of the inflow z_R and the depth of the cold pool z_c are known. If we use h to represent z_c to be consistent with what is commonly used in studies of gravity currents, we can write (76) in the following to a more familiar form:

$$c = U \pm \left(\frac{H-h}{z_R}\right)\sqrt{2bh} = U \pm c_0\left(\frac{H-h}{z_R}\right) \tag{77}$$

where h is the depth of the cold pool on the far side at $x = -L$, and

$$c_0 = \sqrt{2bh} \tag{78}$$

Only the positive root in (77) is relevant since the squall line is assumed to propagate into the inflow by the definition of the inflow.

A few points can be noted from (77)-(78):

(1) The propagation speed is proportional to the square root of the intensity of the cold pool b. In the hypothetical scenario when the depth of the lower inflow z_R is the same as the thickness of the exiting flow,

$$c = U + c_0 \tag{79}$$

This formula is consistent with what was shown in RKW88 without shear or in optimal condition (their Equation 12). In the scenario when the cold pool is thin $h \ll$H and the inflow is deep $z_R \approx H$, (79) is also approximately valid.

(2) Since the cold pool depth h appears in both (77) and (78), the propagation speed increases with the cold pool depth h when it is thinner than the half depth of the system H, but decreases with h when it is thicker. The maximum speed is attained at $h = \frac{H}{2}$ with

$$c_{max} = U + c_0 \frac{1}{2} \frac{H}{z_R} \tag{80}$$

The thinner the lower inflow layer, the larger the maximum speed. This can be understood by the impact of by u_h on p_{z_c} in (72). When the inflow layer thickness z_R is smaller, for a given depth and intensity of the cold pool, the speed of the outflow is smaller according to (64). The slower speed must be caused by a larger pressure gradient force from the left to the right; hence p_{z_c} is larger. This causes higher pressure at the cold pool head, thus faster propagation. For the same reason, the deeper the inflow layer, the faster the wind speed on the exit side, and the lower the dynamic pressure; this lessens the pressure at the cold pool head, reducing the propagation speed.

(3) In the limiting case of no overturning circulation, $z_R = H$,

$$c = U + c_0 \left(1 - \frac{h}{H}\right) \tag{81}$$

Thus, the relative propagation speed is equal to c_0 multiplied by the square root of the non-dimensional depth of the outflow. We will show later that under this condition, h needs to be equal to $H/2$. As a result, the speed is 50% of c_0: $c = U + 0.5\, c_0$.

(4) Even though CAPE is assumed to be zero, we can get some insight on how it might affect the propagation speed. With CAPE, (73) becomes

$$\frac{p_{z_c}}{\rho} = -\frac{1}{2}\, u_h^2 + \text{CAPE}(0, z_c) + \frac{1}{2} u_0^2 \tag{82}$$

Thus, the larger the CAPE of air rising from the surface to the altitude z_c, the larger the pressure p_{z_c}, and therefore, the faster the relative propagation speed of a squall line. $\text{CAPE}(0, z_c)$ may be negative because of CIN when z_c is not sufficiently higher than the LFC. CIN slows the propagation of a squall line. The physical interpretation of the impact of CAPE on the propagation speed is as follows: When CAPE is positive, it accelerates the air flow. The speed of the air flow however is constricted by the mass continuity requirement of the outflow. The air needs to be slowed down, and this can only be accomplished by larger pressure on the exit side. This increases the dynamic pressure at the cold pool head, leading to faster propagation. This interpretation is only a conceptual description CAPE impact on the propagation speed. It is not a real proof since when CAPE is nonzero, the far-side wind speed is no longer constant as described by (64) and the depth of the cold pool as well as the inflow will also adjust.

3.4.3 Momentum constraint

Because the wind speeds are constant on both the right (u_0) and left (u_h) boundaries in the toy model, the perturbation pressure $p(x=-L,z)$ for $z \in [z_c, H]$ is also a constant based on the application of the Bernoulli equation at each height. Therefore $p(x=-L,z) = p_{z_C}$ for $z \in [z_c, H]$. The integrals in the momentum budget equation (56) can thus be directly obtained and the budget becomes the following:

$$(\rho u_h^2 + p_{z_C})(H - z_c) = \rho u_0^2 z_R + (P_{\psi=\psi_R} - P_{\psi=0}) \tag{83}$$

Eliminating p_{z_C} by using (73), we get another relationship between the velocity in the exit flow u_h and the inflow u_0 that is independent of kinematic relationship (64):

$$\frac{1}{2}\rho(u_0^2 + u_h^2)(H - z_c) = \rho u_0^2 z_R + (P_{\psi=\psi_R} - P_{\psi=0}) \tag{84}$$

$P_{\psi=0}$ and $P_{\psi=\psi_R}$ involve the pressure distribution along the internal boundaries. They are not easily available without knowing the outer solutions. But in the present special case of motionless and hydrostatic cold pool, according to (65) the pressure field at the far side in the cold pool for $z \in [0, z_c]$ is

$$p(L,z) = p_{z_c} + \rho b(z_c - z) \tag{85}$$

Since the region is motionless, in the cold pool,

$$p(x,z) = p(L,z) = p\left(x_{\psi=0}, z\right) \tag{86}$$

Substituting (86) and (85) into the definition of $P_{\psi=0}$ in (57), we can get the total pressure acting on the jump flow horizontally by the cold pool as follows:

$$P_{\psi=0} = \int_0^{z_c}[p_{z_c} + \rho b(z_c - z)]dz = p_{z_c} z_c + \frac{1}{2}\rho b z_c^2 \tag{87}$$

p_{z_c} in (87) can be eliminated again by using the Bernoulli equation (73). We then obtain the following:

$$P_{\psi=0} = \frac{1}{2}\rho(u_0^2 - u_h^2)z_c + \frac{1}{2}\rho b z_c^2 \tag{88}$$

We need to know the integrated pressure $P_{\psi=\psi_R}$ along the upper boundary of $\psi = \psi_R$ to completely describe the momentum budget in (84). This requires the knowledge of the overturning circulation, which will be the subject of the next section. For now as an illustrative toy model, we assume $P_{\psi=\psi_R}$=0 as a limiting cases of no overturning circulation or when the pressure acting on the jump flow horizontally by the overturning circulation is small. With this assumption and substituting (88) into (84), we can get

$$\frac{1}{2}\rho(u_0^2 + u_h^2)(H - z_c) = \rho u_0^2 z_R - \frac{1}{2}\rho(u_0^2 - u_h^2)z_c - \frac{1}{2}\rho b z_c^2 \tag{89}$$

Using (74) to replace bz_c by $\frac{1}{2}u_h^2$ in (89) and grouping the terms by the u_h and u_0, we can write (89) as

$$u_h^2\left(H - \frac{3z_c}{2}\right) = u_0^2(2z_R - H) \tag{90}$$

This relationship between u_h and u_0 and the kinematic relationship in (64) both need to be satisfied for the steady-state solution. Eliminating u_h in (90) by using (64), one can get the following constraint on the depth of the cold pool z_c:

$$(H - \frac{3}{2}z_c)\left(\frac{z_R}{H-z_c}\right)^2 u_0^2 = u_0^2(2z_R - H) \tag{91}$$

As a result, z_c must satisfy the following:

$$(H - \frac{3}{2}z_c)\left(\frac{z_R}{H-z_c}\right)^2 = (2z_R - H) \tag{92}$$

Therefore, the depth of the cold pool z_c can be determined from the depth of the inflow z_R. z_R is a property of the overturning circulation, which we will determine in the next section. Assuming the limiting case of $z_R = H$, one can find that the only non-zero solution of (92) is

$$z_c = \frac{H}{2} \tag{93}$$

This is the well-known gravity current depth that has been extensively studied and laboratory confirmed (e.g., Benjamin, 1968; Xu, 1992; Xue, 2007)

The above derivation also allows us to infer the impact of the overturning circulation on the depth of the cold pool. Since the inflow of the overturning circulation is generally high above the surface, the rising air typically has negative CAPE because the LFL cannot be easily reached. As a result, wind speed is reduced by CIN, which corresponds to positive perturbation pressure at the interface of $\psi = \psi_R$, leading to positive value of $P_{\psi=\psi_R}$ in (84). This increases the westward flux of momentum that needs to offset by the cold pool pressure, which implies a deeper cold pool than the case without an overturning circulation.

3.5 Far-Side Solution: General Environmental Conditions

Far-side solutions can be constructed for other simple cases of the environmental inflow and CAPE by setting selected environmental conditions of $U(z_0)$ in (38) and $CAPE(z_0, z)$ in (30). If the cold pool is motionless and hydrostatic, a similar derivation as Section 3.3 will lead to a constraint on the propagation speed of the cold pool. If the pressure force from the overturning circulation is neglected, a similar derivation as Section 3.4 will lead to a constraint on the cold pool depth. MG72 studied the special case of constant shear of the mean flow and simple CAPE in the form of

$$CAPE(z_0, z) = \Gamma(\mathrm{z} - \mathrm{z}_0)$$

Xue (2007) studied the special case of a two-layer environmental flow, in which a layer of constant velocity is above a layer of constant shear and $CAPE(z_0, z) = 0$. To limit the length of this paper, these and other special cases for the jump flow are not discussed here. Instead, we outline the numerical steps to obtain the far-side solutions under general environmental conditions. As pointed out in MG72, even with CAPE as simple as $\Gamma(\mathrm{z} - \mathrm{z}_0)$ and constant shear, analytical form of the far-side solution is not easy to obtain. This is because ψ is no longer a linear function of z_0, and as a result $z_0 = z_0(\psi)$ in (39) is nonlinear, which appears in the denominator in the forcing term F in (41). Therefore, for practical applications, numerical solution of the one-dimensional 2nd-order differential equation (44) is a more efficient option than an analytical solution.

For a motionless cold pool with given input of the inflow depth z_R and total pressure from the overturning circulation $P_{\psi=\psi_R}$, the numerical solution of the far-side jump flow can be obtained by using the following steps:

(1) Prepare for the environmental fields: Calculate buoyancy $\mathrm{B}(z_0, z)$ and $\mathrm{CAPE}(z_0, z)$ from the environmental thermodynamic profile. Calculate the environmental vorticity η_0 by using the third equation in (38).

(2) Take an initial guess of the cold pool height $\mathrm{z_c}$ to start the numerical shooting.

(3) Take an initial guess of the propagation speed c to start the second loop of numerical shooting, then calculate the relative environmental wind $u_0(z_0)$ from the first equation in (38).

(4) Use the inflow wind profile $\mathrm{u_0}(z_0)$ to obtain the profile of the stream function by using the second equation in (38). This gives the mapping between z_0 and ψ and the value of the separating streamline ψ_R in (43).

(5) Take an initial guess of the ψ profile at the far side on the left boundary $x = -L$. The values should be in the range between 0 and ψ_R. The guess can be based on the vorticity profile without consideration of CAPE. Use the guessed ψ at a set of grids z to obtain the corresponding $\mathrm{z_0}$ by using the mapping between $\mathrm{z_0}$ and ψ from step (4) and interpolation.

(6) Use the obtained $\mathrm{z_0}$ to calculate the vorticity forcing on the left-hand side of (44) by interpolation of the environmental fields in step (1) and the known mapping relationship in step (4).

(7) Get the residual of the far-side vorticity equation from the initial guess of ψ by using (44) and the boundary conditions of (45)-(46). Use an iteration method to solve ψ. This determines the far-field stream function. Obtain the wind from the stream function.

(8) Use the Bernoulli equation (37) to obtain the pressure distribution as a function of z. Obtain its value p_{z_c} at z_c. Compare p_{z_c} with the same variable from (71). Use the difference as a residual to iterate on the propagation speed c by repeating steps (3)-(8) until the p_{z_c} converges. The final c in the converged solution gives the propagation speed of the squall line with the given environmental conditions.

(9) Use the wind field from step (7) and pressure field from step (8) to calculate the left-hand side of the momentum equation (56); use $P_{\psi=0}$ from (87) and input $P_{\psi=\psi_R}$ as well as the inflow from step (3) to calculate the right-hand side of equation (56). Iterate on the depth of the cold pool z_c to balance the momentum constraint (56) by repeating steps (2)-(9). The final z_c in the converged solution gives the depth of the cold pool under the given environmental conditions and $z_R, P_{\psi=\psi_R}$. $z_R, P_{\psi=\psi_R}$ will be determined later by using information of the overturning circulation.

If the cold pool has motions in it, $P_{\psi=0}$ needs to be an input variable. The numerical steps are the same as described above up to step (7). For step (8), the pressure relationships (68)-(69) in

the cold pool need to be modified based on the circulation within the cold pool. Equation (71) in step (8) will be replaced by the modified pressure equation. $P_{\psi=0}$ from (87) will be replaced by a direct input of $P_{\psi=0}$ from the cold pool solution. More details will be further discussed in Section 6.2 For step 9. As for the toy model, step (8) constrains the propagation speed; step (9) constrains the cold pool depth.

One may ask what happens if the propagation speed and cold pool depth do not satisfy the constraints described above, or the model solution does not exist. If they are not met, the system cannot be in steady state with flows as in Figure 3. The environmental condition cannot accommodate a steady-state jump flow.

4. The Overturning Flow

4.1 Formulation and Boundary Conditions

The governing equation of the stream function in the region of the overturning flow in Figure 3 is the same as for the jump flow, i.e., equation (40) along with the definition of the forcing in (41). The domain of the solution is the region above the streamline $\psi(x,z) = \psi_R$.

The top and lower boundary conditions are simply

$$\psi(x,H) = \psi_R \tag{94}$$

$$\psi(x,z)|_{z=h_R(x)} = \psi_R \tag{95}$$

At the lower boundary of the interface with the jump flow, the pressure continuity leads to the continuity of wind speed since CAPE along the interface is the same in the overturning circulation and the jump flow. Thus,

$$|\nabla\psi|^2 = |\nabla\psi|^2_{jump\ flow} \quad \text{at } z = h_R(x) \tag{97}$$

The lateral boundary condition at $x = L$ is separated into two portions for the inflow and outflow in $z \in [z_R, H]$. The separation height is denoted as z_s, which is to be determined. Below z_s in the inflow,

$$\psi(x = L, z) = \psi_R + \int_{z_R}^{z} \rho u_0 \, dz \quad \text{for } z \in [z_R, z_s] \tag{98}$$

or equivalently,

$$\psi(x = L, z) = \int_{0}^{z} \rho u_0 \, dz \quad \text{for } z \in [0, z_s] \tag{99}$$

In the outflow for $z \in [z_s, H]$, the boundary condition is provided by the far-side solution.

There is at least one stagnation point in the solution domain at the upper boundary, where velocity equals to zero. This is property of the inner solution of the overturning circulation.

4.2 Far-Side Solution, Layer Thickness

By definition, at the separation height z_s of the inflow and outflow at $x = L$, $u_0(z_s) = 0$; z_s is the steering height of the squall line. If the propagation speed c is known, z_s can be calculated from the environmental flow by

$$U(z_s) = c \tag{100}$$

When the environmental wind is not monotonic with height, (100) may have more than one solution. The overturning circulation therefore could have multiple layers of inflow and outflow. Such cases are not considered in this paper since the these have not been shown as common features of squall lines in the published literature.

It is theoretically possible that $U(z) < c$ at all altitudes so that no steering level exists. In this case, there would be no overturning circulation. The squall line propagates forward relative to the environmental flow at all height. The case of $U(z) > c$ violates the assumption of an inflow into the squall line from the right side, but it can be considered as a horizontal flip with inflow from the left side, thus the same discussions can be applied. A special case is when U is constant above a layer in the lower troposphere with shear. This setup has been used in many idealized simulations in the literature. In this case, either the steering level is in the sheared layer, or no overturning circulation exists. It is not possible for the model to admit an overturning solution with exactly the same constant U as the steering speed.

The far-side stream function below z_s at $x = L$ is determined by the incoming flow described in (98). Above it, the stream function satisfies the same one-dimensional 2nd-order differential equation of (44), but with the following boundary conditions

$$\psi(z = z_s) = \psi_s \tag{101}$$

$$\psi(z = H) = \psi_R \tag{102}$$

ψ_s and ψ_R are obtained from the incoming flow in (98) if z_R is known.

We are now ready to settle z_R. With known CAPE, the stream function above z_s is completely determined by the flow below z_s, the mass continuity requirement in the overturning circulation constrains z_R by the following:

$$\int_{z_R}^{z_s} \rho u_0(z_0) dz_0 + \int_{z_s}^{H} \rho u dz = 0 \tag{103}$$

An example of the specific procedure to obtain z_R will be given in the next subsection. But the following conclusion can be drawn from the formulation: Once the propagation speed is known, the environmental wind profile and CAPE in the overturning circulation completely determine the thickness and other properties of the overturning flow. Wind profile and CAPE elsewhere, as well as the specifics of the jump flow and cold pool circulation do not directly impact the far-field outflow of the overturning circulation. They impact the outflow only indirectly by affecting the propagation speed of the system.

4.3 Body Force on the Jump Flow

The momentum budget of the total overturning circulation is the same as (55) for the jump flow except that the domain is the region above the streamline $\psi(x,z) = \psi_R$ in Figure 3. Using the boundaries of the overturning flow, the budget can be written as follows:

$$\int_{z_R}^{z_s} \rho u_0^2 dz + \int_{z_s}^{H} \rho u^2(x=L) dz + \int_{z_s}^{H} p(L,z)\, dz - P_{\psi=\psi_R} = 0 \tag{104}$$

After the pressure field in the outflow is replaced by using the Bernoulli equation (37), we can obtain the following:

$$P_{\psi=\psi_R} = \int_{z_R}^{z_s} \rho u_0^2 dz + \int_{z_s}^{H} \rho u^2 dz + \int_{z_s}^{H} \left[\frac{u_0^2}{2} - \frac{u^2}{2} + CAPE(z_0,z)\right] dz \tag{105}$$

The far-side solution at $x = L$ is described in the previous subsection. Thus, the total pressure acting horizontally on the jump flow by the overturning circulation $P_{\psi=\psi_R}$, or the body force of the overturning flow on the jump flow, is determined. When the term in the bracket of (105) is small, this equation shows that the pressure perturbation is positive and proportional to the square of the lateral flow speed. The positive value of $P_{\psi=\psi_R}$ is consistent with what can be inferred from the equation of motion (23) written in the natural coordinate system: For the streamlines to turn clockwise as from the inflow to the outflow in the overturning circulation, the horizontal pressure gradient force needs to point to the right of the trajectories. The gradient is proportional to the square of the inflow speed, so is the body force.

4.4 A toy model

We use the special case of constant wind shear in a neutral atmosphere as a toy model to illustrate how the formulated overturning circulation may be applied. In this case,

$$CAPE(z_0,z) = 0 \quad \text{and} \quad U(z) = U_0 + \alpha z \tag{106}$$

where U_0 is the ground level speed of environmental wind; α is the shear. We further assume that ρ is constant.

If the propagation speed of the squall line is c, which is determined in the model of the jump flow, the steering height z_s can be calculated according to (100):

$$z_s = \frac{1}{\alpha}(c - U_0) \tag{107}$$

z_s must be larger than zero and less than H, or else there is no overturning circulation.

The inflow in the propagating reference frame is

$$u_0 = U_0 + \alpha z - c = u_{00} + \alpha z \tag{108}$$

where u_{00} is the relative inflow speed at the surface. The steering level can be written in terms of u_{00} as:

$$z_s = -\frac{1}{\alpha} u_{00} \tag{109}$$

In the inflows of both the jump flow and the overturning circulation below z_s, according to the second equation in (38) the stream function is

$$\psi(x = L, z) = \int_0^z \rho u_0(z)\, dz = \rho u_{00} z + \frac{1}{2}\rho\alpha z^2 \quad \text{for } z \in [0, z_s] \tag{110}$$

Hence,

$$\psi_R = \rho u_{00} z_R + \frac{1}{2}\rho\alpha z_R^2 \tag{111}$$

and

$$\psi_s = \rho u_{00} z_s + \frac{1}{2}\rho\alpha z_s^2 \tag{112}$$

Since the inflow vorticity equals to α and there is no CAPE, the far-side vorticity equation (44) in the outflow becomes a linear 2nd-order differential equation:

$$\frac{\partial^2 \psi}{\partial z^2} = \alpha\rho \tag{113}$$

The following solution would satisfy the above equation and the boundary conditions (102) at $z = H$:

$$\psi(z) = \psi_R + \frac{\alpha\rho}{2}(z - z_R)(z - H) \quad \text{for } z \in [z_s, H] \tag{114}$$

Enforcing the boundary condition at $z = z_s$ constrains z_R:

$$\psi_s = \psi_R + \frac{\alpha\rho}{2}(z_s - z_R)(z_s - H) \tag{115}$$

z_R is thus obtained by substituting ψ_s and ψ_R in (111) and (112) into (115), which gives

$$z_R = -\frac{2}{\alpha} u_{00} - H \tag{116}$$

where the value of the surface inflow speed u_{00} is negative. This formal derivation can be more intuitively obtained as follows: The thickness of the outflow is $H - z_s$. Since the shear is the same above and below the steering level due to the vorticity conservation, the inflow of the overturning circulation should have the same thickness as the outflow. Therefore

$$z_s - z_R = H - z_s \tag{117}$$

Thus,

$$z_R = 2z_s - H \tag{118}$$

Substituting (109) into the above equation, one gets the same answer as (116).

In this toy model, the velocity in the outflow is a mirror image of the inflow with an opposite sign. This means the pressure perturbation in the outflow is zero because CAPE is zero. Thus, the body force of the overturning circulation on the jump flow is:

$$P_{\psi=\psi_R} = \alpha^2 \int_{z_R}^{z_s} (z - z_s)^2 dz + \alpha^2 \int_{z_s}^{H} (z - z_s)^2 dz = \frac{1}{12}\alpha^2 (H - z_R)^3 \tag{119}$$

The integrated pressure is proportional to the square of the shear and the cube of the thickness of the overturning circulation. The overturning circulation can impact the global properties of the squall line through $P_{\psi=\psi_R}$ and z_R. Thus, the wind distribution in the middle and upper

troposphere may also play important roles in the propagation and other properties of the squall line.

4.5 General Environmental Condition

With the insights from the toy model and knowledge from the jump flow, we outline the numerical steps to obtain the far-side solutions of both the overturning circulation and the jump flow under general conditions of the environmental wind and CAPE. The following steps can be inserted into what have been described in Section 3.4 after step (3) for the jump flow.

(1) Obtain the steering height z_s by using (100).
(2) Obtain the stream function ψ(z) below z_s by using the inflow speed in (99). This gives the mapping relationship between ψ and the origination altitude z_0 for $z \in [z_R, z_s]$: $\psi = \psi(z_0)$ and $z_0 = z(\psi)$
(3) Take an initial guess of the ψ profile of the outflow above z_s. The guess can be based on an antisymmetric wind profile with respect to z_s without consideration of CAPE. Use the value of ψ at $z = H$ to obtain the initial guess of z_R. Other guess values should be in the range between ψ_R and ψ_s.
(4) Use the guessed ψ for $z \in [z_s, H]$ and the mapping relationship in step (2) to obtain the corresponding z_0.
(5) Use the obtained z_0 to calculate the vorticity forcing on the right-hand side of (44) by using (41).
(6) Get the residual of the far-side vorticity equation (44) from the initial guess of ψ and boundary conditions of (101)-(102). Use an iteration method to solve ψ so that the residual converges to zero. This determines the far-field stream function of the outflow and the wind profile. The final z_R corresponding to the converged solution is the separation altitude between the jump flow and the overturning flow.
(7) Use (105) and the converged solution in step (6) to obtain the body force of pressure $P_{\psi=\psi_R}$.

The derived z_R and $P_{\psi=\psi_R}$ from the above calculation are then used as input to continue the iteration for the jump flow in Section 3.4 to determine the propagation speed *c* and the cold pool height on the far left side, subject to input of the pressure force from the backside of the jump flow $P_{\psi=0}$.

If desired, the pressure in the outflow of the overturning circulation can be diagnosed from the motion by using the Bernoulli equation (37):

$$\frac{p}{\rho} = \frac{u_0^2(z_0)}{2} - \frac{u^2(z)}{2} + CAPE(z_0, z) \tag{120}$$

where z_0 is mapped to z by using the value of the stream function ψ at z from the far-side solution in step (6) and the mapping relation in step (2); $u(z)$ is obtained from ψ.

5. The Backside Flow

5.1 Formulation

We use the terms of backside flow, descending-rear-inflow, and cold pool flow interchangeably to describe the circulation below the jump flow. We have shown before (Section 3.4.2) that a hydrostatic and motionless cold pool relative to the propagating squall line is a special solution of the backside flow. However, this assumption is no longer valid if CAPE depends on both the initial and arrival altitudes. Furthermore, as the squall line propagates, the motionless solution implies a very large shear near the surface where the ground level speed is zero due to friction, which is not realistic.

The backside flow can be passive, just as a response to the falling precipitation from the jump flow and the associated pressure field. It can also be active with its own inflow that forces vertical motion. In the latter, the squall line should be within a region of strong large-scale convergence so that the backside large-scale inflow can catch the propagating squall line. The flow patten is then more like an isolated plume than the typical pattern of squall line in the schematic Figure 3. We limit our discussion to the passive type.

In our model, we assume that buoyancy is a source of positive vorticity or clockwise circulation on the backside. The flow is assumed to be forced by cooling due to evaporation and melting of hydrometers falling from the jump flow, by the loading of hydrometers, or by the pressure field directing downward. When air below the jump flow descends, it may be negatively buoyant or positively buoyant if the evaporation of available condensates and the loading of hydrometers are not sufficient to balance the adiabatic warming. Without knowing the details of the diabatic heating and hydrometer distributions in the descending flow, we assume that the generalized CAPE is known, be it negative or positive, acknowledging that the evaporative cooling and hydrometer loading depend on a variety of external factors such as the number and size of falling particles which further relate to the aerosols and cloud microphysics.

We denote the buoyancy in the cold pool region by $B_b(z_0, z)$ with a subscript "b" and the corresponding CAPE by $CAPE_b(z_0, z)$ to distinguish them from the buoyancy $B(z_0, z)$ and $CAPE(z_0, z)$ in the other two flow regions. We also assume that at the far side of $x = -L$, the atmosphere is hydrostatic with known cold pool intensity. Thus, at $x = -L$,

$$\frac{p(z)}{\rho} = \frac{p_{z_c}}{\rho_{z_c}} - \int_z^{z_c} B_c(z)\mathrm{dz} \quad \text{for } z \in [0, z_c] \tag{121}$$

where p_{z_c} is the pressure at the interface height $z = z_c$ obtained from the jump flow; $B_c(z)$ is the cold pool intensity at $x = -L$. By definition, $B_c(z) = B_b(z, z)$.

The governing equation of the stream function of the backside circulation is (40), the same as that for the jump flow and overturning circulation, except that in the calculation of $F(\psi, z)$ in (41), $CAPE_b(z_0, z)$ is used.

The top and lower boundary conditions of the backside flow are,

$$\psi(x,z)|_{z=h_0(x)} = 0 \text{ for } x \in [-L, 0] \tag{122}$$

$$\psi(x,z)|_{z=0} = 0 \text{ for } x \in [-L, 0] \tag{123}$$

where $h_0(x)$ is the free boundary between the jump flow and the backside flow. The pressure continuity across the interface after the use of the Bernoulli equation gives an additional boundary condition to constrain the interface height at $z = h_0(x)$:

$$-\frac{1}{2\rho}|\nabla\psi|^2 + \rho\left[\mathrm{CAPE_b}(z_c, z) + \frac{1}{2}u_{z_c}^2\right] = -\frac{1}{2\rho}|\nabla\psi|^2_{jump\ flow} + \rho\left[\mathrm{CAPE}(0, z) + \frac{1}{2}u_0^2(0)\right] \tag{124}$$

Here we have used different forms of CAPE for the backside flow and the ascent jump flow, since the air moves in opposite directions along the interface and so their associated heating processes can be different.

To formulate the boundary condition on the left side, as with the jump flow and the overturning circulation, we seek far-side solution. This is discussed next.

5.2 Far-Side Solution and Degree of Freedom

We introduce z_b as the height that separates the inflow and outflow on the backside as indicated in the schematic Figure 3. At this height, the storm relative velocity is zero. We denote the coordinate of the origination altitudes of the inflow as $z_0 \in [z_b, z_c]$ and the outflow coordinate altitudes as $z \in [0, z_b]$. The far-side vorticity equation is written in the following form by using (25):

$$\frac{\partial u}{\partial z} = \frac{\partial u_0}{\partial z_0} - \frac{1}{u_0(z_0)}\int_z^{z_0} \frac{\partial B_b(z_0, z)}{\partial z_0} dz \tag{125}$$

in which the ending points of the integral have been reversed to change from the lower exiting altitude z to the higher inflow altitude z_0 instead of from the origination altitude to the exiting altitude. (125) can be rearranged as follows:

$$\frac{\partial u}{\partial z} = \frac{\partial u_0}{\partial z}\frac{\partial z}{\partial z_0} - \frac{1}{u_0(z_0)}\int_z^{z_0} \frac{\partial B_b(z_0, z)}{\partial z_0} dz \tag{126}$$

The mass continuity requirement can be written as:

$$\frac{\partial z}{\partial z_0} = -\frac{u_0(z_0)}{u(z)} \tag{127}$$

where we used the convention that dz and dz_0 are both positive when pointing upward and that the wind directions above and below z_b are opposite to each other. Substituting (127) into (126) leads to

$$\frac{\partial u}{\partial z} = -\frac{1}{2\,u(z)}\frac{\partial u_0^2(z_0)}{\partial z} - \frac{1}{u(z_0)}\int_z^{z_0}\frac{\partial B_b(z_0,z)}{\partial z_0}dz \tag{128}$$

Using the Bernoulli equation (37) to write the inflow kinetic energy as the difference between the exiting energy and the work by the buoyancy and the pressure, we can get:

$$\frac{u_0^2(z_0)}{2} = \frac{u^2(z)}{2} + \frac{p(z)}{\rho(z)} - \frac{p(z_0)}{\rho(z_0)} - CAPE_b(z_0,z) \tag{129}$$

Since on the far side the cold pool is hydrostatic, by substituting the pressure in (121) into (130), we can express $u_0(z_0)$ as a function of $u(z)$ in the following:

$$\frac{u_0^2(z_0)}{2} = \frac{u^2(z)}{2} - \int_z^{z_0} B_c(z)\mathrm{dz} - CAPE_b(z_0,z) = \frac{u^2(z)}{2} + \Psi(z_0,z) \tag{130}$$

or

$$\mathrm{u_0(z_0)} = \sqrt{u^2(z) + 2\Psi(z_0,z)} \tag{131}$$

where

$$\Psi(z_0,z) = -\int_z^{z_0} B_c(z)\mathrm{dz} - CAPE_b(z_0,z) \tag{132}$$

$\Psi(z_0,z)$ can be calculated based on the buoyancy distribution at the far side and CAPE from the environmental condition.

Substituting (130) and (131) into (128) with some minor manipulations, we can get

$$\frac{\partial u}{\partial z} = -\frac{1}{2}\frac{\partial \Psi(z_0,z)}{\partial z} - \frac{1}{2\sqrt{u^2(z)+2\Psi(z_0,z)}}\int_z^{z_0}\frac{\partial B_b(z_0,z)}{\partial z_0}dz \tag{133}$$

Substituting (131) into (127), we can get

$$\frac{\partial z_0}{\partial z} = -\frac{u(z)}{\sqrt{u^2(z)+2\Psi(z_0,z)}} \tag{134}$$

The about two equations (133)-(134) can be integrated for $u(z)$ and $z_0(z)$ from $z = 0$ upward to $z = z_b$, with the initial condition at surface to be

$$\begin{pmatrix} u \\ z_0 \end{pmatrix}\Big|_{z=0} = \begin{pmatrix} u_{b0} \\ z_c \end{pmatrix} \tag{135}$$

where u_{b0} is the velocity immediately above the surface that is to be determined, and z_c is the cold pool height discussed in the section of the jump flow.

At $z = z_b$, the solutions must satisfy the following:

$$\begin{pmatrix} u \\ z_0 \end{pmatrix}\Big|_{z=z_b} = \begin{pmatrix} 0 \\ z_b \end{pmatrix} \tag{136}$$

(136) constrains the surface velocity u_{b0}, and the separation height z_b. Once $u(z)$ is known, $u_0(z_0)$ can be obtained from (131). This leads to the complete far-side solution of $\psi(x = -L, z)$ as the lateral boundary condition of the backside flow.

It is somewhat surprising that the backside solution can be determined with so few information. The following physical interpretation may provide some insight: The pressure field at the far side is given by the hydrostatic equation. The Bernoulli equation therefore gives a known relationship between the velocity at an inflow height with the outflow height on the same streamline. The vorticity source in the cold pool is determined by the buoyancy or CAPE that depend on the altitudes, and thus the vertical shear of the wind speed in the inflow and outflow are related to each other. The mass continuity requirement dictates that there is only one far-side solution that can fit in the range of $z \in [0, z_c]$ with zero net mass flux.

The motionless solution is a special case of $B_b(z_0, z) = B_c(z)$, which leads to

$$\Psi(z_0, z) = 0 \tag{137}$$

in (132) and thus the boundary conditions in (136) lead to the following solution:

$$\frac{\partial u}{\partial z} = 0 \text{ and } u(z) = 0 \tag{138}$$

The above formulation implies that the cold pool circulation at the far side is primarily determined by the distribution of the buoyancy in the backside. The environmental wind impacts it indirectly through other global properties of the squall line, including the dynamic pressure, the propagation speed, and the cold pool height.

Depending on the distribution of $B_b(z_0, z)$ on the backside, it is possible that the buoyancy creates negative vorticities immediately below the jump flow, a counter-clockwise circulation above the cold pool circulation. This is analogous to an overturning circulation sandwiched between the cold pool flow and the jump flow. In such case, velocity on the far-side at the top of the cold pool $x = -L, z = z_c$ is expected to be continuous in z. This velocity can be obtained from the jump flow. It gives the condition to constrain the depth of the embedded overturning circulation. The boundary conditions (135) and (136) can be modified accordingly. Such scenario would eliminate the discontinuity of far-side velocity between the descending cold pool flow and the ascending jump flow in the setup of Figure 3, which could create Kelvin-Helmholtz instability with billowing eddies. Since the scenario depends on the specification of $B_b(z_0, z)$, we only point out it here and leave further study to future numerical simulations.

As mentioned before, due to surface friction, the ground speed of wind should be zero. The relative speed of the surface wind u_{b0} in the cold pool should be equal to $-c$ where c is the propagation speed of the squall line. This is equivalent to imposing an external condition on the far-field flow immediately above the ground. We suspect that this is a constraint on the distribution of buoyancy $B_b(z_0, z)$ in the steady-state solution, but we do not have a proof of it yet.

Given the backside flow, the total pressure acting on the jump flow by the backside flow can be obtained by using the integrated momentum budget. When (55) is applied to the region of the backside flow, we get

$$P_{\psi=0} = \int_{z_b}^{z_c} \rho u_0^2 dz + \int_0^{z_b} \rho u^2 dz + \int_0^{z_c} p(x=-L,z)dz \tag{139}$$

Substituting the hydrostatic pressure (121) into the last term in (139), we get

$$P_{\psi=0} = \int_{z_b}^{z_c} u_0^2 dz + \int_0^{z_b} u^2 dz + \int_0^{z_c} \left(\rho(z)[\frac{p_{z_c}}{\rho_{z_c}} - \int_z^{z_c} B_c(z')\mathrm{d}z']\right) dz \tag{140}$$

The third term in (140) is the total pressure force at the far side, which is positive, while $P_{\psi=0}$ is the total horizontal force at the interface. The difference of these two forces is equal to the momentum flux at the far side.

For numerical solution under generalized environmental conditions, we can append the following steps after the calculation steps for the overturning flow described in Section 4.5:

(1) Take an initial guess of u_{b0} as initial condition in (135). Integrate (133) and (134) upward by using the initial condition of (135) to obtain the wind $u(z)$ and $z_0(z)$.
(2) Iterate on u_{b0} so that the boundary conditions (136) are met. The final z_b is the separation height between the inflow and outflow on the backside. Obtain the stream function from the wind by using the second equation in (38). Obtain the mapping between ψ and z_0. Calculate $u_0(z_0)$ by using (131).
(3) Calculate $P_{\psi=0}$ in (140). Use it as input of the iteration for the jump flow described in Section 3.4.

5.3 A Toy Model

As an illustration, we present a toy model in which the buoyancy function in the backside $B_b(z_0,z)$ is written as

$$B_b(z_0,z) = B + \Gamma(\mathrm{z}-\mathrm{z_b})(z-z_0) \tag{141}$$

where B is a constant, representing the intensity of the far-side cold pool, and $B_c(z) = B$. We also assume that the air density is a constant. Since for descending air, $z_0 > z$, (141) describes a scenario that in the inflow region $z > z_b$, the descending air has negative buoyance relative to B due to melting or evaporation, while in the outflow region, $z < z_b$, and the descending air has positive buoyance relative to B. This form is used only for illustrative purpose, bearing in mind that actual distribution could be very different and complex.

Using (141) in the definition of CAPE in (35), we have

$$CAPE_b(z_0,z) = \int_{z_0}^{z} [B + \Gamma(\mathrm{z}-\mathrm{z_b})(z-z_0)]dz \tag{142}$$

or

$$CAPE_b(z_0,z) = -B(z_0-z) + \frac{\Gamma}{3}(z-z_0)^3 + \frac{\Gamma}{2}(z_0-z_b)(z-z_0)^2 \tag{143}$$

From (132), we have

$$\Psi(z_0, z) = -\frac{\Gamma}{3}(z - z_0)^3 - \frac{\Gamma}{2}(z_0 - z_b)(z - z_0)^2 \tag{144}$$

By using (141), the integral factor of the vorticity forcing in the last term of (133) is

$$-\int_z^{z_0} \frac{\partial B_b(z_0,z)}{\partial z_0} dz = \int_z^{z_0} \Gamma(\mathrm{z} - \mathrm{z_b}) dz = \frac{\Gamma}{2}(z_0 - z_b)(z + z_0 - 2z_b) \tag{145}$$

Substituting (144) and (145) into (133), we get

$$\frac{\partial u}{\partial z} = \frac{\Gamma}{2}\left[(z - z_0)^2 + (z_0 - z_b)(z - z_0) + \frac{(z_0 - z_b)(z + z_0 - 2z_b)}{2\sqrt{u^2(z) - \frac{2\Gamma}{3}(z - z_0)^3 - \Gamma(z_0 - z_b)(z_0 - z)^2}}\right] \tag{146}$$

Substituting (144) into (134), we get

$$\frac{\partial z_0}{\partial z} = -\frac{u(z)}{\sqrt{u^2(z) - \frac{2\Gamma}{3}(z - z_0)^3 - \Gamma(z_0 - z_b)(z_0 - z)^2}} \tag{147}$$

(146) and (147) along with the boundary conditions (135) and (136) give a far-side solution of the cold pool flow. Here the only input variables from the jump flow are the height of the cold pool z_c that is used in the boundary condition in (135).

Figure 4 shows an example the calculated far-side solution by using (146) -(147) and an iteration method. In the calculation, we have assumed Γ in the buoyancy specification (141) to be $\Gamma = 3.0 \times 10^{-8}$ kg m/s^2/ m^2, z_c to be 6 km as the cold pool depth. Figure 4(a) is the second term in $B_b(z_0, z)$ on the right-hand side of (141) in the unit 10^{-2} kg m/s^2, plotted as a function of z_0 and z. It is the deviation of buoyance from the buoyancy at $x = -L$ since only the deviation matters to the circulation. The abscissa is the originating altitude of air parcels z_0 with values of the x-axis reversed. The ordinate is the arriving altitude z. For example, when the originating altitude is $z_0 = 6$ km, the range of the arrival altitudes is $z \in [0,6]$. The calculated separation altitude from the iteration is $z_b = 2.1$ km. The buoyancy deviation is negative above z_b and positive below z_b as specified in (141).

Figure 4(b) is $CAPE_b(z_0, z)$ from z_0 to z corresponding to Figure 4a, calculated from the second and third terms on the right-hand side of (143) with the unit of 10 J. $CAPE_b(z_0, z)$ for a descending parcel with initial condition at z_0 above z_b is positive because buoyancy is negative. Passing downward after z_b, $CAPE_b$ of an air parcel decreases because of positive buoyancy. Figure 4(c) gives the factor of the vorticity forcing by the buoyancy in (145). The positive value is because $CAPE_b$ of a parcel originating from a higher altitude is larger than that from a lower altitude, as seen by comparing the CAPE value in the horizontal direction of z_0 in the figure for the same arrival altitude z when it is larger than z_b.

The solution of the far-side flow calculated from (146) and (131) is shown in Figure 4(d). The wind speed relative to the propagating squall line in the outflow at the surface is about 20 m/s. The outflow is concentrated below about 2 km, while the inflow is primarily within in a

shallower layer from about 4.5 km to 6 km. For the specified $B_b(z_0, z)$ in this toy model, there will be a large shear between the backside flow and the jump flow. As stated before, such shear will create Kelvin-Helmholtz instability. The ensuing eddies will render the state-state assumption invalid. The toy model presented here is to illustrate how far-side solution can be constructed that satisfies the vorticity equation and the boundary conditions.

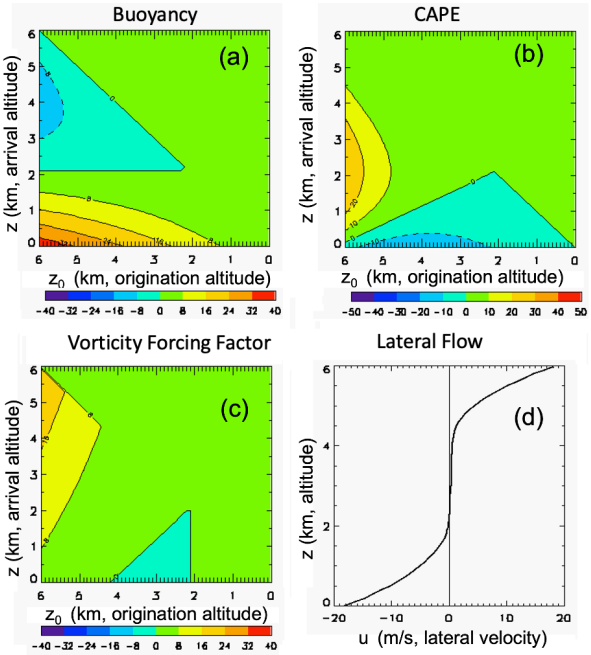

Figure 4. (a)-(c) Specified buoyancy (unit in 10^{-2} kg m/s^2), calculated CAPE (unit in 10J), and a factor of the vorticity source in the toy-model on the backside. The abscissa is the origination altitude of a parcel. The ordinate is the arrival altitude. The values of the x-axis is reversed. (d) The far-side flow speed (unit in m/s).

6. The Coupled Flows and Global Properties

With the overturing circulation and backside flow formulated in Section 4 and 5, we are ready to revisit the constraints on the propagation speed and cold pool height discussed in Section 3 for the jump flow. They are part of the global properties of the whole solution of the squall line.

At or immediately above the surface, the vertical velocity is zero, so the horizontal momentum equation (54) of the steady state in the propagating system is

$$\frac{\partial}{\partial x}\left(\frac{1}{2}\rho u^2 + p\right) = 0 \tag{148}$$

Here I have used the advective form of the momentum equation rather than the flux form, since only in the advection form the term associated with the vertical velocity is zero at the surface. Integrating (148) from the far left $x = -L$ to the far right $x = L$ and considering that the pressure perturbation in the inflow at the far right is zero, we get

$$\frac{1}{2}\rho u_{00}^2 = \frac{1}{2}\rho u_{b0}^2 + p(x=-L, z=0) \tag{149}$$

where u_{00} is the speed of the inflow at the surface; u_{b0} is the speed of the backside flow at the surface. Substituting the backside pressure at the surface by using the hydrostatic relation on the far side in (121), we get

$$\frac{1}{2}u_{00}^2 = \frac{1}{2}u_{b0}^2 + \frac{p_{z_c}}{\rho_{z_c}} - \int_0^{z_c} B_c(z)\mathrm{dz} \tag{150}$$

Using (73) to eliminate p_{z_c}, we can obtain the following after some minor rearrangements:

$$u_{z_c}^2 = u_{b0}^2 - 2\int_0^{z_c} B_c(z)\mathrm{dz} \tag{151}$$

Since $u(z) = U(z) - c$, the above equation constrains the propagating speed after u_{z_c} and u_{b0} are determined.

In the special case of the toy model in Section 3.4, the environmental flow and density are constant, and the backside flow is motionless, $u_{b0} = 0$, with

$$u_{z_c} = \frac{z_R}{H - z_c} u_{00} \tag{152}$$

(151) becomes

$$\left(\frac{z_R}{H - z_c} u_{00}\right)^2 = \sqrt{-2\int_0^{z_c} B_c(z)\mathrm{dz}} \tag{153}$$

This is the same as (75) that gives the propagation speed of the jump flow in (77).

Under general conditions, since by the definition of the cold pool,

$$B_c(z) < 0 \tag{154}$$

(151) implies that the exit flow at the top of the cold pool in the jump flow must satisfy the following, otherwise there would be no propagation.

$$u_{z_c}^2 > u_{b0}^2 \tag{155}$$

(150) also indicates that the cold pool circulation act to increase the propagation speed of the squall line. An intuitive physical interpretation is that when there is circulation in the cold pool, there is an additional pressure gradient at the cold pool head to force the flow to the backside. This increases the head pressure and causes it to propagate faster to the right.

Although the mean environmental flow and CAPE do not explicitly appear in constraint on the propagation speed implied in (151), they impact the cold pool height z_c and the relationships between $u_{z_c}$and u_{b0} with u_{00}, which can play substantial roles in affecting the propagation speed as in the special case given by (153).

We next revisit the constraint on the cold pool height z_c to extend what was discussed for the jump flow in Section 3.3.4. By summing up the total momentum equations of the three flows (56), (105) and (139), we can get the following total momentum equation:

$$\left[\int_0^{z_b} u^2 dz + \int_{z_b}^{z_c} u_0^2 dz + \int_0^{z_c} p dz\right]_{\substack{x=-L \ in \\ backside\ flow}} + \left[\int_{z_c}^{H} \rho u^2\, dz + \int_{z_c}^{H} p dz\right]_{\substack{x=-L \ in \\ jump\ flow}}$$
$$= \left[\int_0^{z_R} \rho u_0^2 dz_0\right]_{\substack{x=L \ in \\ jump\ flow}} + \left[\int_{z_R}^{z_s} \rho u_0^2 dz + \int_{z_s}^{H} \rho u^2 dz + \int_{z_s}^{H} p\, dz\right]_{\substack{x=L \ in \\ overturning\ flow}} \quad (156)$$

The pressure field of the backside flow in (156) is obtained by the hydrostatic equation in (121) ; those for the other two flows can be obtained from the Bernoulli equation (37) by using the wind speed of the inflow and exit flow and CAPE. (156) is the constraint on the cold pool height z_c as discussed as a special case in Section 3.4.3.

The horizontal body force acting on the jump flow $P_{\psi=0}$ by the overturning circulation has been given in (140). The body force acting on the jump flow $P_{\psi=\psi_R}$ by the backside flow, according to (56), is as follows:

$$P_{\psi=\psi_R} = P_{\psi=0} + \left[\int_{z_c}^{H} \rho u^2\, dz + \int_{z_c}^{H} p dz\right]_{\substack{x=-L \ in \\ jump\ flow}} - \left[\int_0^{z_R} \rho u_0^2 dz_0\right]_{\substack{x=L \ in \\ jump\ flow}} \quad (157)$$

The above descriptions complete our formulation of the squall line flows and their constraints. For easy reference, we summarize the governing equations, boundary conditions and the momentum budget in Table 1 for the stream functions of the three flows. The numbers in the parentheses are the equation numbers in the text. The equations and boundary conditions for the far-side solutions are summarized in Table 2.

Table 1 Governing equation, boundary conditions, and momentum budget in the three flows. The numbers in the parenthesis at the end of each equation are the equation numbers in the text.

governing Equation	$\frac{\partial^2\psi}{\partial x^2} + \frac{\partial^2\psi}{\partial z^2} + \frac{1}{H_s}\frac{\partial\psi}{\partial z} = F(\psi, z)$ (40) $F(\psi, z) = \frac{\rho^2(z)}{\rho[z_0(\psi)]}\{\eta_0[z_0(\psi)] + \frac{1}{u_0[z_0(\psi)]} G[z_0(\psi), z]\}$ (41) $\frac{\partial\psi}{\partial z_0} = \rho(z_0)u_0(z_0)$ (19), $\eta_0 = \frac{\partial u_0}{\partial z_0}$ (38), $G(z_0, z) = -\frac{\partial CAPE(z_0,z)}{\partial z_0}$ (32)		
flows	jump flow (ascending front-to-rear flow)	Overturning flow	backside or cold pool flow (descending rear inflow)
solution domain	$x \in [-L\ , L]$ $z \geq h_0(x), \psi[x, h_0(x)] = 0;$ $z \leq h_R(x), \psi[x, h_R(x)] = \psi_R$	$x \in [-L\ , L]$ $z \geq h_R(x), \psi[x, h_R(x)] = \psi_R;$ $z \leq H$	$x \in [-L\ , 0]$ $z \geq 0$; $z \leq h_0(x), \psi[x, h_0(x)] = 0$
upper boundary condition	$\psi[x, h_R(x)] = \psi_R$ (49); $\|\nabla\psi\|^2 = \|\nabla\psi\|^2_{overturning\ flow}$ at $z = h_R(x)$ (97)	$\psi(x, H) = \psi_R$ (94)	$\psi[x, h_0(x)] = 0$ (122); $-\frac{1}{2\rho}\|\nabla\psi\|^2 +$ $\rho\left[\mathrm{CAPE_b}(z_c, z) + \frac{1}{2}u_{z_c}^2\right] =$ $\left\{-\frac{1}{2\rho}\|\nabla\psi\|^2 +\right.$ $\rho\left[\mathrm{CAPE}(0, z) +\right.$ $\left.\left.\frac{1}{2}u_0^2(0)\right]\right\}_{jump\ flow}$ (124)
lower boundary condition	$\psi[x, h_0(x)] = 0$ (48); $-\frac{1}{2\rho}\|\nabla\psi\|^2 + \rho\left[\mathrm{CAPE}(0, z) +\right.$ $\left.\frac{1}{2}u_0^2(0)\right] = \left\{-\frac{1}{2\rho}\|\nabla\psi\|^2 +\right.$	$\psi[x, h_R(x)] = \psi_R$ (95)	$\psi(x, 0) = 0$ (123)

	$\rho\left[\text{CAPE}_{\text{b}}(z_c,z)+\frac{1}{2}u_{z_c}^2\right]\}_{backside\ flow}$ at $z=h_0(x)$ (124)	$\lvert\nabla\psi\rvert^2=\lvert\nabla\psi\rvert^2_{jump\ flow}$ at $z=h_R(x)$ (97)	
boundary condition at $x=-L$	Far-side solution	N/A	Far side solution
boundary condition at $x=L$	$\psi(x=L,z)=\psi_R+\int_0^z\rho_0u_0\,dz$ for $z\,\epsilon\,[0,z_R]$ (43)	$\psi(x=L,z)=\psi_R+\int_{z_R}^z\rho_0u_0\,dz$ for $z\,\epsilon\,[z_R,z_s]$ (98); Far side solution for $z\,\epsilon\,[z_s,H]$	N/A
Momentum budget	$\left[\int_{z_c}^H\rho u^2\,dz+\int_{z_c}^H pdz\right]_{x=-L\ in\ jump\ flow}=\left[\int_0^{z_R}\rho u_0^2dz_0\right]_{x=L\ in\ jump\ flow}+(P_{\psi=\psi_R}-P_{\psi=0})$ (56)	$P_{\psi=\psi_R}=\left[\int_{z_R}^{z_s}\rho u_0^2dz+\int_{z_s}^H\rho u^2dz+\int_{z_s}^H p\,dz\right]_{x=L\ in\ overturning\ flow}$ (105)	$P_{\psi=0}=\left[\int_0^{z_b}u^2dz+\int_{z_b}^{z_c}u_0^2dz+\int_0^{z_c}pdz\right]_{x=-L\ in\ backside\ flow}$ (140)

Table 2 Governing equation, boundary conditions of the far-side solution in the three flows. The numbers in the parenthesis at the end of each equation are the equation numbers in the text.

flow	jump flow (ascending front-to-rear flow)	overturning flow	backside or cold pool flow (descending rear inflow)
governing equations	$\frac{d^2\psi}{dz^2}+\frac{1}{H_s}\frac{d\psi}{dz}=F(\psi,z)$ (44) $\frac{\partial\psi}{\partial z_0}=\rho(z_0)u_0(z_0),\quad\eta_0=\frac{\partial u_0}{\partial z_0}$ (38) $z_0=z_0(\psi)$ (39) $F(\psi,\text{z})=\frac{\rho^2(z)}{\rho[z_0(\psi)]}\{\eta_0[z_0(\psi)]+\frac{1}{u_0[z_0(\psi)]}G[z_0(\psi),\text{z}]\}$ (41) $G(z_0,z)=-\frac{\partial CAPE(z_0,z)}{\partial z_0}$ (32)		$\frac{\partial u}{\partial z}=-\frac{1}{2}\frac{\partial\Psi(z_0,z)}{\partial z}-\frac{1}{2\sqrt{u^2(z)+2\Psi(z_0,z)}}G(z_0,z)$ (146) $\frac{\partial z_0}{\partial z}=-\frac{u(z)}{\sqrt{u^2(z)+2\Psi(z_0,z)}}$ (147) $\Psi(z_0,z)=-\int_z^{z_0}B_c(z)\text{dz}-CAPE_b(z_0,z)$ (144)
solution domain	outflow $x=-L$ $z\,\epsilon\,[z_c,H]$	outflow $x=L$ $z\,\epsilon\,[z_s,H]$	outflow $x=-L, z\,\epsilon\,[0,z_b]$ inflow $x=-L, z\,\epsilon\,[z_b,z_c]$
upper boundary condition	$\psi(H)=\psi_R$ (49)	$\psi(z_s)=\psi_s$ (94)	$\binom{u}{z_0}\Big\rvert_{z=z_b}=\binom{0}{z_b}$ (136)
lower boundary condition	$\psi(z_c)=0$ (48)	$\psi(H)=\psi_R$ (95)	$\binom{u}{z_0}\Big\rvert_{z=0}=\binom{u_{b0}}{z_c}$ (135)
toy model	Section 3.4	Section 4.4	Section 5.3

The global properties include, but not limited to, the following variables:

- c propagation speed
- z_c depth of the cold pool
- z_R depth of the jump flow
- z_s steering-level height
- z_b separation height of the inflow and outflow in the cold pool at the backside
- ψ_R mass flux of the jump flow
- ψ_s total mass flux of the jump flow and overturning circulation
- ψ_B mass flux of the backside flow

- u_{b0} surface flow speed in the cold pool on the far side
- $P_{\psi=0}$ horizontal pressure body force between cold pool and jump flow
- $P_{\psi=\psi_R}$ horizontal pressure body force between overturning and jump flows

All heights and ψ_R are marked in the schematic Figure 3. Constraints on each of these properties described in the previous three sections are summarized in Table 3.

Table 3 Constraints on the global properties. The numbers in the parenthesis at the end of each equation are the equation numbers in the text.

global properties	c propagation speed z_c cold pool height z_R depth of the jump flow z_s steering-level height z_b separation height of the backside inflow and outflow	ψ_R mass flux of the jump flow ψ_s total mass flux of the jump flow and overturning circulation ψ_B mass flux of the backside flow u_{b0} backside surface flow speed $P_{\psi=0}$ horizontal pressure force between cold pool and jump flow $P_{\psi=\psi_R}$ horizontal pressure force between overturning and jump flows
constraint on propagation speed c	$(1-\frac{\rho_0}{\rho_{z_c}})u_{00}^2 = u_{b0}^2 - u_{z_c}^2 - 2\int_0^{z_c} B_c(z)\mathrm{dz}$ (151)	
constraint on cold pool height z_c	$\left[\int_0^{z_b} u^2dz + \int_{z_b}^{z_c} u_0^2dz + \int_0^{z_c} pdz\right]_{\substack{x=-L\ in\\ backside\ flow}} + \left[\int_{z_c}^{H} \rho u^2\, dz + \int_{z_c}^{H} pdz\right]_{\substack{x=-L\ in\\ jump\ flow}}$ $= \left[\int_0^{z_R} \rho u_0^2 dz_0\right]_{\substack{x=L\ in\\ jump\ flow}} + \left[\int_{z_R}^{z_s} \rho u_0^2 dz + \int_{z_s}^{H} \rho u^2 dz + \int_{z_s}^{H} p\, dz\right]_{\substack{x=L\ in\\ overturning\ flow}}$ (156)	
constraint on jump flow depth z_R	$\int_{z_R}^{z_s} \rho u_0(z_0)dz_0 + \int_{z_s}^{H} \rho u dz = 0$ (103)	
steering level z_s	$U(z_s) = c$ (100)	
constraint on separation height of the backside inflow and outflow z_b	$\begin{pmatrix} u \\ z_0 \end{pmatrix}\Big\|_{z=z_b} = \begin{pmatrix} 0 \\ z_b \end{pmatrix}$ (136)	
mass flux of the jump flow ψ_R	$\psi_R = \int_0^{z_R} \rho u_0(z_0)\, dz_0$ (42)	
total mass flux of the jump flow and overturning circulation ψ_s	$\psi_s = \psi_R + \int_{z_R}^{z_s} \rho u_0\, dz$ (98)	
mass flux of the backside flow ψ_B	$\psi_B = \int_{z_b}^{z_c} \rho u\, dz$ (38)	
backside surface flow speed u_{b0}	$\begin{pmatrix} u \\ z_0 \end{pmatrix}\Big\|_{z=z_b} = \begin{pmatrix} 0 \\ z_b \end{pmatrix}$ (136)	
horizontal pressure force between cold pool and jump flow $P_{\psi=0}$	$P_{\psi=0} = \left[\int_0^{z_b} u^2dz + \int_{z_b}^{z_c} u_0^2dz + \int_0^{z_c} pdz\right]_{\substack{x=-L\ in\\ backside\ flow}}$ (140)	
horizontal pressure force between overturning and jump flows $P_{\psi=\psi_R}$	$P_{\psi=\psi_R} = \left[\int_{z_R}^{z_s} \rho u_0^2 dz + \int_{z_s}^{H} \rho u^2 dz + \int_{z_s}^{H} p\, dz\right]_{\substack{x=L\ in\\ overturning\ flow}}$ (105)	

7. Discussion

The formulation presented in this paper is limited to steady state flows in the reference frame of a propagating squall line. In the real world or in numerical simulations with prescribed initial conditions, gravity waves co-exist with the quasi-steady circulation of squall lines. Whether the formulations in this paper can represent the mean mesoscale scale circulation depends on whether the gravity waves are averaged out by canceling the their flows within the period of the waves. The frequency of gravity waves within the mean flow is approximately

$$\omega \approx \frac{kN}{\sqrt{(k^2+m^2)}} \tag{158}$$

where ω is the frequency of the wave and k, m are horizontal and vertical wave numbers. When the horizontal wave number is comparable to the vertical wave number $m \approx k$, $\omega \approx \frac{N}{\sqrt{2}}$. typically values of N is 0.01 s^{-1} in the free atmosphere without consideration of adiabatic heating (e.g., Figure 3 in Pandya and Durran 1996), which leads to a period of about 15 minutes. This is much shorter than the lifetime of a squall line. Thus, the steady-state solution may be representative of the time-averaged flows of a real squall line outside the cores. But this remains to be numerically confirmed.

The formulation is limited to two dimensions. Even for squall lines, they often propagate in directions both perpendicular to and parallel with the squall line. The flow pattern presented in this paper is for the projection of the time-averaged flows in the plane perpendicular to the squall line. Whether the parallel propagation of squall lines is merely an advection of the mean wind at the steering level is an open question. Additionally, given a vertical profile of the mean wind of unidirectional shear, the orientation of the squall line relative to the mean wind needs to be determined since this affects the speed of the inflow. It is possible that the orientation can be inferred from the environmental condition where squall lines are optimally trigged. The RKW88 theory provides such a candidate, as has been shown in Abramian et al. (2022). The near-field solution of the flows as formulated in this paper may also provide conditions in which the conversion of energy from the CAPE and shear is maximized. This remains to be investigated.

The model is formulated for flow configuration as in Figure 3 that does not include all likely flow patterns in squall lines. An example is the elevated inflow over a stably stratified boundary layer due to surface infrared radiative cooling and intrusion of the cold pool flow below the inflow, as in cases of nocturnal bores (Haghi et al., 2019; Haghi and Durran 2021). Extension of the formulation to include such configuration can be made by modifying the solution domain of the backside circulation in Figure 3 if dissipative processes play minor roles. Another example is the rotor circulation within the backside circulation near the cold pool head or at the separation region of the jump current and the overturning circulation. Such solutions are possible in the model under certain combinations of the environmental conditions of the buoyancy field, CAPE and the mean wind if they are not the result of dissipative processes. But these remain to be

demonstrated at least numerically. On the backside of the squall line system, as discussed in Section 5.2, buoyancy may create negative vorticity or a counter-clockwise circulation that lies immediately below the jump flow above the cold pool flow. Since this depends on the specific form of the buoyancy distribution, it is only briefly discussed in this paper.

While most observed squall lines take the form of Figure 1 with trailing stratiform clouds in the jump flow, other types of systems have been also observed (e.g., Parker and Johnson 2000). These include convective line with leading stratiform precipitation and convective line with rear inflow (e.g., Parker and John 2004). It is possible that the overturning circulation in the model described here can accommodate the leading stratiform precipitation, and that the rear-fed squall lines can be viewed as retreating system relative to the inflow. Sometimes the cold pool is very weak or does not exist, in principle the same control equations of the stream functions can be used, but the formulation will require appropriate modification based on the flow patterns.

The model presented assumes inviscid flow. Turbulent mixing and other non-dissipative processes are prevalent in convective storms and clouds. The theory is therefore limited to strong and long-lasting steady state systems in which the irreversible processes play minor roles relative to those by nonlinear transport and pressure gradient force at the scale comparable to the depth of the domain sizes of the solutions discussed in the paper.

The model assumes that buoyancy distribution is a known function of the initial and final altitudes of a parcel. In the ascending flows, this may be a reasonable assumption. In the descending flow, the buoyancy is tightly coupled with the jump flow and descending flow in which cloud and precipitation microphysics as well as radiative heating may play important roles in determining the buoyancy. The specified buoyancy distribution is thus an idealization to isolate the dynamics from the forcing.

Despite these limitations, the formulations have provided insights on the coherence of the squall lines. Their global properties have small degree of freedoms. When the environmental wind and CAPE in the inflow are known, the cold pool strength completely determine its height, the propagation speed of the squall line, the mass fluxes of the different flows, and other global properties of a squall line as described in Table 3. Possible applications include the prediction of these properties, for example, the propagation speed of the squall line, when the environmental conditions are known and the cold pool properties can be estimated based on profiles of humidity and temperature. If the cold pool strength or the backside CAPE can be described by a single variable of its macro property, such as a constant value of intensity, then when the propagation speed is observed from radar or satellite, all other properties including the backside CAPE of the squall lines can be inferred.

The formulation also provides a framework for squall lines to be parameterized in climate model by using resolvable large-scale environmental conditions. The model can be used to check

whether large-scale environmental condition can support a steady-state squall line. The model also allows the calculation of the mass fluxes of the mesoscale inflow, updrafts and downdrafts by using parameterized forms of the cold pool buoyancy. The mass fluxes of the ascending flow can be used to estimate the flux of water vapor and thus intensity of precipitation. A more robust parameterization could include the parameterization of the cold pool buoyancy by using the flow field from the near-field solution of the model described in Table 1.

8. Summary

We have formulated the mathematical governing equations and boundary conditions of the interlocked flows for steady-state two-dimensional squall lines. The flows include the ascending front-to-rear flow, the front overturning circulation, and the descending-rear-inflow or backside flow. These are summarized in Table 1. The governing equations of the stream functions are 2^{nd} order nonlinear elliptic equations with environmental wind and CAPE as input and with free internal boundaries. Far-side solutions are formulated as one-dimensional 2^{nd}-order different equations. Toy models and their solutions are presented for each flow type to illustrate the physical processes controlling the flow patterns. Procedures of numerical calculations are outlined for general environmental conditions.

The formulations lead to constraints of the global properties of the squall lines. They include the propagation speed, depth of the cold pool, depth of the ascending front-to-rear flow, the steering level, the separation height of the backside inflow and outflow in the cold pool, the mass fluxes of the ascending front-to-rear flow, the front overturning circulation, and the descending inflow or backside flow, the surface flow speed in the cold pool on the far side, and the horizontal pressure body forces between the interlocked flows. These constraints are summarized in Table 3. Given environmental wind and CAPE that is generalized to include buoyancy in the cold pool, these properties can be determined. Thus the squall lines have small degree of freedom in their dynamic organization, due to the conservation requirements of mass, momentum, energy and vorticity within in a propagating system that maintains a steady state.

We have also discussed the limitations and potential applications of the theory. Numerical and observational verification of the theory and its potential applications are needed. These are being pursued in follow-up research.

Conflict of Interest

The authors declare no conflicts of interest relevant to this study.

Data Availability Statement

This is a theoretical paper that does not involve data.

Acknowledgements:

I wish to thank Brian Colle and Shaocheng Xie for their valuable comments on an earlier draft of the paper.

Appendix A Pressure, vorticity and the Bernoulli equations

A.1 The Pressure Equation

The equations of motion (1)-(2) are written as

$$\frac{\partial u}{\partial t} + \vec{V} \cdot \nabla u = -\frac{1}{\rho}\frac{\partial p}{\partial x} + F_u \tag{A1}$$

$$\frac{\partial w}{\partial t} + \vec{V} \cdot \nabla w = -\frac{1}{\rho}\frac{\partial p}{\partial z} + B + F_w \tag{A2}$$

Here ρ is assumed to be only a function of height.

By taking $\frac{\partial \rho \times (A1)}{\partial x} + \frac{\partial \rho \times (A2)}{\partial z}$ and using the anelastic mass continuity equation (3), we can get

$$\nabla^2 p = -\nabla \cdot \left(\rho \vec{V} \cdot \nabla \vec{V}\right) + \frac{\partial \rho B}{\partial z} + \left(\frac{\partial \rho F_u}{\partial x} + \frac{\partial \rho F_w}{\partial z}\right) \tag{A3}$$

The first term on the left-hand side can be manipulated as the following:

$$\begin{aligned}
\nabla \cdot \left(\rho \vec{V} \cdot \nabla \vec{V}\right) &= \frac{\partial(\rho \vec{V} \cdot \nabla \mathrm{u})}{\partial x} + \frac{\partial(\rho \vec{V} \cdot \nabla \mathrm{w})}{\partial z} = \rho \vec{V} \cdot \nabla\left(\frac{\partial u}{\partial x} + \frac{\partial w}{\partial z}\right) + \frac{\partial(\rho \vec{V})}{\partial x} \cdot \nabla \mathrm{u} + \frac{\partial(\rho \vec{V})}{\partial z} \cdot \nabla \mathrm{w} \\
&= -\rho \vec{V} \cdot \nabla\left(\frac{1}{\rho}\frac{d\rho}{dt}\right) + \rho\left(\frac{\partial u}{\partial x}\frac{\partial u}{\partial x} + \frac{\partial w}{\partial x}\frac{\partial u}{\partial z}\right) + \left(\frac{\partial \rho u}{\partial z}\frac{\partial w}{\partial x} + \frac{\partial \rho w}{\partial z}\frac{\partial w}{\partial z}\right) \\
&= -\rho \vec{V} \cdot \nabla\left(\frac{w}{\rho}\frac{\partial \rho}{\partial z}\right) + \rho\left(\frac{\partial u}{\partial x}\frac{\partial u}{\partial x} + \frac{\partial w}{\partial x}\frac{\partial u}{\partial z}\right) + \rho\left(\frac{\partial u}{\partial z}\frac{\partial w}{\partial x} + \frac{\partial w}{\partial z}\frac{\partial w}{\partial z}\right) + \left(u\frac{\partial w}{\partial x} + w\frac{\partial w}{\partial z}\right)\frac{\partial \rho}{\partial z} \\
&= -\rho \vec{V} \cdot \nabla\left(\frac{w}{\rho}\frac{\partial \rho}{\partial z}\right) + \rho\left[\left(\frac{\partial u}{\partial x}\right)^2 + \left(\frac{\partial w}{\partial z}\right)^2 + 2\frac{\partial u}{\partial z}\frac{\partial w}{\partial x}\right] + \frac{\partial \rho}{\partial z}\vec{V} \cdot \nabla w \\
&= -\frac{\partial \rho}{\partial z}\vec{V} \cdot \nabla w - w\rho \vec{V} \cdot \nabla\left(\frac{1}{\rho}\frac{\partial \rho}{\partial z}\right) + \rho\left[\left(\frac{\partial u}{\partial x}\right)^2 + \left(\frac{\partial w}{\partial z}\right)^2 + 2\frac{\partial u}{\partial z}\frac{\partial w}{\partial x}\right] + \frac{\partial \rho}{\partial z}\vec{V} \cdot \nabla w \\
&= -\rho w^2 \frac{\partial^2 ln\rho}{\partial z} + \rho\left[\left(\frac{\partial u}{\partial x}\right)^2 + \left(\frac{\partial w}{\partial z}\right)^2 + 2\frac{\partial u}{\partial z}\frac{\partial w}{\partial x}\right]
\end{aligned} \tag{A4}$$

Substituting (A4) into (A3), one can get the perturbation pressure equation (5).

A.2 The Vorticity Equation and Approximation

By taking $\frac{\partial(A1)}{\partial z} - \frac{\partial(A2)}{\partial x}$, we can get

$$\frac{\partial \eta}{\partial t} + \vec{V} \cdot \eta + \frac{\partial \vec{V}}{\partial z} \cdot \nabla u - \frac{\partial \vec{V}}{\partial x} \cdot \nabla w = -\frac{\partial p}{\partial x}\frac{\partial}{\partial x}\left(\frac{1}{\rho}\right) - \frac{\partial B}{\partial x} + F_\eta \tag{A5}$$

Neglecting the change of the pressure gradient force with height due to density change, (A5) becomes

$$\frac{d\eta}{dt} + \frac{\partial \vec{V}}{\partial z} \cdot \nabla u - \frac{\partial \vec{V}}{\partial x} \cdot \nabla w = -\frac{\partial B}{\partial x} + F_\eta \tag{A6}$$

Since

1263
$$\frac{\partial \vec{V}}{\partial z}\cdot\nabla u-\frac{\partial \vec{V}}{\partial x}\cdot\nabla w=\frac{\partial u}{\partial z}\frac{\partial u}{\partial x}+\frac{\partial w}{\partial z}\frac{\partial u}{\partial z}-\frac{\partial u}{\partial x}\frac{\partial w}{\partial x}-\frac{\partial w}{\partial x}\frac{\partial w}{\partial z}$$
$$=\left(\frac{\partial u}{\partial z}-\frac{\partial w}{\partial x}\right)\left(\frac{\partial u}{\partial x}+\frac{\partial w}{\partial z}\right)=-\eta\frac{1}{\rho}\frac{d\rho}{dt} \quad \text{(A7)}$$

1264 (A6) can be written as

$$\frac{d\eta}{dt}-\eta\frac{1}{\rho}\frac{d\rho}{dt}=-\frac{\partial B}{\partial x}+F_\eta \quad \text{(A8)}$$

1265 This is equivalent to the following:

$$\frac{1}{\rho}\frac{d\eta}{dt}+\eta\frac{d}{dt}\left(\frac{1}{\rho}\right)=-\frac{1}{\rho}\frac{\partial B}{\partial x}+\frac{1}{\rho}F_\eta \quad \text{(A9)}$$

1266 which leads to the vorticity equation (12).

1267

1268 **A.3 The Bernoulli's Equation and Approximation**

1269

1270 By taking $u\times(A1)+w\times(A2)$, we get

$$\frac{\partial}{\partial t}\left(\frac{V^2}{2}\right)+\vec{V}\cdot\left(\frac{V^2}{2}\right)=-\frac{1}{\rho}\vec{V}\cdot\nabla p+wB+uF_u+wF_w$$
$$=-\vec{V}\cdot\nabla\left(\frac{p}{\rho}\right)+p\vec{V}\cdot\nabla\left(\frac{1}{\rho}\right)+wB+F_E \quad \text{(A10)}$$

1271 This can be written as

$$\frac{D}{Dt}\left(\frac{V^2}{2}\right)=-\frac{D}{Dt}\left(\frac{p}{\rho}\right)-\frac{\partial}{\partial t}\left(\frac{p}{\rho}\right)+p(\vec{V}\cdot\nabla\alpha)+B\frac{Dz}{Dt} \quad \text{(A11)}$$

1272 where α is the specific volume. Under steady-state and with assumption that work performed by
1273 the perturbation pressure is small so that the third term on the left-hand side of (A11) can be
1274 neglected, rearrangement of (A11) leads to the Bernoulli equation (14).

1275

1276 **Appendix B Horizontal Vorticity Equation and Momentum Equation in Natural System**

1277

1278 **B.1 The Equivalence**

1279

1280 Using the Stokes' theorem, we write the horizontal vorticity defined in (13) as circulation per
1281 unit area in a natural coordinate system with $\vec{s}$ and $\vec{n}$ as the coordinates (see Figure B1 for
1282 definitions of symbols used below). We have

$$\eta=\frac{1}{A}\oint_A\vec{V}\cdot d\vec{l}=\lim_{\substack{\Delta s\to 0\\ \Delta n\to 0}}\frac{1}{\Delta s\Delta n}\left(\int_a^b \mathrm{V}\mathrm{ds}+\int_c^d \mathrm{V}\mathrm{ds}\right)$$
$$=\lim_{\substack{\Delta s\to 0\\ \Delta n\to 0}}\frac{1}{\Delta s\Delta n}\left(\int_a^b \mathrm{V}\mathrm{ds}-\int_d^c \mathrm{V}\mathrm{ds}\right)$$
$$=\lim_{\substack{\Delta s\to 0\\ \Delta n\to 0}}\frac{1}{\Delta s\Delta n}\left[\mathrm{V}\Delta s-\left(\mathrm{V}+\frac{\partial V}{\partial n}\Delta n\right)(\Delta s-d\Delta s)\right] \quad \text{(B1)}$$

$$= \lim_{\substack{\Delta s\to 0\\ \Delta n\to 0}} \left(-\frac{\partial V}{\partial n} + \mathrm{V}\frac{\mathrm{d}(\Delta s)}{\Delta s \Delta n}\right) = \lim_{\substack{\Delta s\to 0\\ \Delta n\to 0}} \left(-\frac{\partial V}{\partial n} + \mathrm{V}\frac{\Delta\alpha}{\Delta s}\right)$$

Thus,

$$\eta = -\frac{\partial V}{\partial n} + \frac{\mathrm{V}}{\mathrm{R}} \tag{B2}$$

where R is the curvature radius defined as

$$R^{-1} = \kappa = \lim_{\Delta s\to 0} \frac{\Delta\alpha}{\Delta s} \tag{B3}$$

κ is the curvature defined as the change of the angle of the normal direction corresponding to a unit change of the arc length.

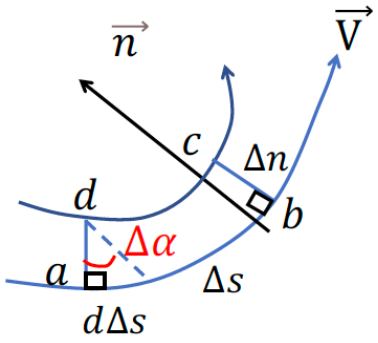

Figure B1. Circulation and horizontal vorticity in the x-z plane

If the streamline is written as

$$z = f(x) \tag{B4}$$

then the normal direction is :

$$\vec{n} = \left(-\frac{f_x'}{\sqrt{1+f_x'^2}}, \frac{1}{\sqrt{1+f_x'^2}}\right) \tag{B5}$$

Write the vorticity equation (22) by using its form in the natural system (B2), we have the following

$$\frac{1}{\rho}\left(-\frac{\partial V}{\partial n} + \frac{\mathrm{V}}{\mathrm{R}}\right) = \frac{1}{\rho_0}\left(-\frac{\partial V_0}{\partial n_0} + \frac{\mathrm{V}_0}{\mathrm{R}_0}\right) + \int_{z_0}^{z} \frac{\partial B(z_0,z)}{\partial z_0}\frac{1}{\rho_0 u_0}\, dz \tag{B6}$$

where the subscript "0" denotes initial location at the far boundary. Since for initial parcels located at the lateral boundary, $p_0 = B(z_0, z_0) = 0$, $u_0 = -V_0$ for the inflow, and $\mathrm{R}_0 = \infty$, (B10) can be written as

$$\frac{1}{\rho}\left(-\frac{\partial V}{\partial n} + \frac{\mathrm{V}}{\mathrm{R}}\right) = -\frac{1}{\rho_0}\frac{\partial V_0}{\partial n_0} - \frac{1}{\rho_0 V_0}\int_{z_0}^{z} \frac{\partial B(z_0,z)}{\partial z_0}\, dz \tag{B7}$$

Taking the chain role of derivative to dn by dn_0 (equivalent to dz_0) and considering V as a function of z_0 and z, we can write the vorticity as

$$-\frac{\partial V}{\partial n} + \frac{\mathrm{V}}{\mathrm{R}} = -\frac{\partial V}{\partial n_0}\frac{\partial n_0}{\partial n} - \frac{\partial V}{\partial z}\frac{\partial z}{\partial n} + \frac{\mathrm{V}}{\mathrm{R}} = -\frac{\partial V}{\partial n_0}\frac{\rho V}{\rho_0 V_0} - \frac{\partial V}{\partial z}\frac{1}{\sqrt{1+f_x'^2}} + \frac{\mathrm{V}}{\mathrm{R}}$$

$$= -\frac{\rho}{2\rho_0 V_0}\frac{\partial V^2}{\partial n_0} - \frac{1}{2}\frac{\partial V^2}{\partial z}\frac{1}{V\sqrt{1+f_x'^2}} + \frac{\mathrm{V}}{\mathrm{R}} \tag{B8}$$

where we have used the mass continuity equation $\rho V dn = \rho_0 V_0 dn_0$. Using the Bernoulli equation (17) to substitute V^2 on the right hand of (B8), we have the following

$$-\frac{\partial V}{\partial n} + \frac{\mathrm{V}}{\mathrm{R}} = -\frac{\rho}{\rho_0 V_0}\frac{\partial}{\partial n_0}\left[\frac{1}{2}V_0^2 + \frac{p_0}{\rho_0} + \int_{z_0}^{z} B(z_0, z)\, dz - \frac{p}{\rho}\right] - \frac{\partial}{\partial z}\left[\frac{1}{2}V_0^2 + \frac{p_0}{\rho_0} + \int_{z_0}^{z} B(z_0, z)\, dz - \frac{p}{\rho}\right]\frac{1}{V\sqrt{1+f_x'^2}} + \frac{\mathrm{V}}{\mathrm{R}}$$

$$= -\frac{\rho}{\rho_0}\frac{\partial V_0}{\partial n_0} - \frac{\rho}{\rho_0 V_0}\left[\int_{z_0}^{z}\frac{\partial B(z_0,z)}{\partial z_0}\, dz - \frac{\partial}{\partial n_0}\left(\frac{p}{\rho}\right)\right] - \left[B(z,z) + \frac{\partial}{\partial z}\left(\frac{p}{\rho}\right)\right]\frac{1}{V\sqrt{1+f_x'^2}} + \frac{\mathrm{V}}{\mathrm{R}} \quad \text{(B9)}$$

Substituting (B9) into the vorticity equation (B7), we can get

$$-\frac{1}{\rho_0}\frac{\partial V_0}{\partial n_0} - \frac{1}{\rho_0 V_0}\left[\int_{z_0}^{z}\frac{\partial B(z_0,z)}{\partial z_0}\, dz - \frac{\partial}{\partial n_0}\left(\frac{p}{\rho}\right)\right] - \frac{1}{\rho}\left[B(z,z) + \frac{\partial}{\partial z}\left(\frac{p}{\rho}\right)\right]\frac{1}{V\sqrt{1+f_x'^2}} + \frac{1}{\rho}\frac{\mathrm{V}}{\mathrm{R}}$$

$$= -\frac{1}{\rho_0}\frac{\partial V_0}{\partial n_0} + \frac{1}{\rho_0}\frac{\mathrm{V}_0}{\mathrm{R}_0} - \frac{1}{\rho_0 V_0}\int_{z_0}^{z}\frac{\partial B(z_0,z)}{\partial z_0}\, dz \quad \text{(B10)}$$

Cancelling the terms on the right and left-hand sides of (B10), we have the following,

$$\frac{1}{\rho_0 V_0}\frac{\partial}{\partial n_0}\left(\frac{p}{\rho}\right) - \frac{1}{\rho}\left[B(z,z) - \frac{\partial}{\partial z}\left(\frac{p}{\rho}\right)\right]\frac{1}{V\sqrt{1+f_x'^2}} + \frac{1}{\rho}\frac{\mathrm{V}}{\mathrm{R}} = 0 \quad \text{(B11)}$$

Using $\rho V dn = \rho_0 V_0 dn_0$ again in the first term, we have

$$\frac{1}{\rho V}\frac{\partial}{\partial n}\left(\frac{p}{\rho}\right) - \frac{1}{\rho}\left[B(z,z) - \frac{\partial}{\partial z}\left(\frac{p}{\rho}\right)\right]\frac{1}{V\sqrt{1+f_x'^2}} + \frac{1}{\rho}\frac{\mathrm{V}}{\mathrm{R}} = 0 \quad \text{(B12)}$$

Using the normal vector (B5), we get

$$\frac{1}{\rho V}\frac{f_x'}{\sqrt{1+f_x'^2}}\frac{\partial}{\partial x}\left(\frac{p}{\rho}\right) - \frac{1}{\rho}\left[B(z,z) - \frac{\partial}{\partial z}\left(\frac{p}{\rho}\right)\right]\frac{1}{V\sqrt{1+f_x'^2}} + \frac{1}{\rho}\frac{\mathrm{V}}{\mathrm{R}} = 0 \quad \text{(B13)}$$

After rearrangement, (B17) becomes the following

$$\left[-\nabla\left(\frac{p}{\rho}\right) + B\vec{k}\right]\cdot\vec{n} = \frac{\mathrm{V}^2}{\mathrm{R}} \quad \text{(B14)}$$

Using the approximation that the vertical change of the pressure gradient force is primarily caused by the pressure change rather than the density change, which is the same approximation to obtain the vorticity equation, (B14) becomes (23).

B.2 Calculation of Streamlines from Curvature

If the curvature radius R is known from using the specified forces in (23) and (24), the streamlines can be obtained by using its relationship with $f(x)$. Length Δs in (B3) corresponding to an increment in Δx is $\sqrt{(1+f_x'^2)}\,\Delta x$. Thus,

$$\Delta\alpha = |\Delta\vec{n}| = \left|\frac{d\vec{n}}{dx}\right|\Delta x = \left|\frac{d\vec{n}}{dx}\right|\frac{1}{\sqrt{1+f_x'^2}}\ \Delta s \quad \text{(B15)}$$

Using (B5), we have

$$\frac{d\vec{n}}{dx} = \left(-\frac{f''_{xx}}{\left(1+f_x'^2\right)\sqrt{1+f_x'^2}}, -\frac{f'_x f''_{xx}}{\left(1+f_x'^2\right)\sqrt{1+f_x'^2}}, \right) \tag{B16}$$

Thus,

$$\left|\frac{d\vec{n}}{dx}\right| = \frac{f''_{xx}}{\left(1+f_x'^2\right)} \tag{B17}$$

Substitution (B17) into (B15) and use the definition in (B3), we can get the familiar expression of curvature as in following:

$$\kappa = \mathrm{R}^{-1} = \frac{1}{\sqrt{1+f_x'^2}}\left|\frac{d\vec{n}}{dx}\right| = \frac{f''_{xx}}{\left(1+f_x'^2\right)^{3/2}} \tag{B18}$$

f''_{xx} from (B18) can then be used along with initial conditions of f and $f'_x = 0$ at the lateral boundary to obtain $f(x)$ in (B4) by integration with x.

References

Abramian, Sophie, Muller, Caroline, and Risi, Camille, 2022, "Shear-Convection Interactions and Orientation of Tropical Squall Lines" Geophysical Research Letters Vol. 49, No. 1, 1944-8007.

Alfaro, D. A., & Khairoutdinov, M. (2015). Thermodynamic Constraints on the Morphology of Simulated Midlatitude Squall Lines, Journal of the Atmospheric Sciences, 72(8), 3116-3137. Retrieved Apr 9, 2022, from https://journals.ametsoc.org/view/journals/atsc/72/8/jas-d-14-0295.1.xml

Benjamin, B. T., 1968: Gravity current and related phenomena. *J. Fluid Mech.*,**31,** 209–248.

Bryan, G. H., & Rotunno, R. (2014). Gravity Currents in Confined Channels with Environmental Shear, *Journal of the Atmospheric Sciences*, *71*(3), 1121-1142. Retrieved Apr 5, 2022, from https://journals.ametsoc.org/view/journals/atsc/71/3/jas-d-13-0157.1.xml

Christopoulos, C., & Schneider, T. (2021). Assessing biases and climate implications of the diurnal precipitation cycle in climate models. *Geophysical Research Letters*, 48, e2021GL093017. https://doi.org/10.1029/2021GL093017

Fan, J., et al. (2017), Cloud-resolving model intercomparison of an MC3E squall line case: Part I—Convective updrafts, *J. Geophys. Res. Atmos.*, 122, 9351– 9378, doi:10.1002/2017JD026622.

Feng, Z., Leung, L. R., Liu, N., Wang, J., Houze, R. A., Li, J., et al. (2021a). A global high-resolution mesoscale convective system database using satellite-derived cloud tops, surface precipitation, and tracking. Journal of Geophysical Research: Atmospheres, 126, e2020JD034202. https://doi. org/10.1029/2020JD034202

Feng, Z., Song, F., Sakaguchi, K., & Leung, L. R. (2021b). Evaluation of mesoscale convective systems in climate simulations: Methodological development and results from MPAS-CAM over the U.S. Journal of Climate, 34(7), 2611–2633. https://doi.org/10.1175/JCLI-D-20-0136.1

Haghi, K. R., & Durran, D. R. (2021). On the Dynamics of Atmospheric Bores, *Journal of the Atmospheric Sciences*, *78*(1), 313-327. Retrieved Apr 5, 2022, from https://journals.ametsoc.org/view/journals/atsc/78/1/jas-d-20-0181.1.xml

Haghi, K. R., and Coauthors, 2019: Bore-ing into nocturnal convection. *Bull. Amer. Meteor. Soc.*, **100**, 1103–1121, https://doi.org/10.1175/BAMS-D-17-0250.1.

Houze, R. A. (2004), Mesoscale convective systems, *Rev. Geophys.*, 42, RG4003, doi:10.1029/2004RG000150.

Houze, 2018: 100 years of research on mesoscale convective systems. A Century of Progress in Atmospheric and Related Sciences: Celebrating the American Meteorological Society Centennial, Meteor. Monogr., No. 59, Amer. Meteor. Soc., https://doi.org/ 10.1175/AMSMONOGRAPHS-D-18-0001.1.

Klemp, J. B., 1987: Dynamics of tornadic thunderstorms. *Annu. Rev. Fluid Mech*, **19 ,** 369–402.

Lin, Y., Dong, W., Zhang, M., Xie, Y., Xue, W., Huang, J., & Luo, Y. (2017). Causes of model dry and warm bias over central US and impact on climate projections. Nature Communications, 8. doi:10.1038/s41467-017-01040-2

Liu, C., Shige, S., Takayabu, Y. N., & Zipser, E. (2015). Latent heating contribution from precipitation systems with different sizes, depths, and intensities in the tropics. Journal of Climate, 28(1), 186–203. https://doi.org/10.1175/JCLI-D-14-00370.1

Moncrieff, M.W. and Green, J.S.A. (1972), The propagation and transfer properties of steady convective overturning in shear. Q.J.R. Meteorol. Soc., 98: 336-352. https://doi.org/10.1002/qj.49709841607.

Moncrieff, M.W. and Miller, M.J. (1976), The dynamics and simulation of tropical cumulonimbus and squall lines. Q.J.R. Meteorol. Soc., 102: 373-394. https://doi.org/10.1002/qj.49710243208

Moncrieff, M. W., 1978: The dynamical structure of two-dimensional steady convection in constant vertical shear. *Quart. J. Roy. Meteor. Soc.*, **104**, 543–568, https://doi.org/10.1002/qj.49710444102.

Moncrieff, M. W., 1981: A theory of organised steady convection and its transport properties. *Quart. J. Roy. Meteor. Soc.*, **107**, 29–50, https://doi.org/10.1002/qj.49710745103.

Moncrieff, M. W., 1992: Organized convective systems: Archetypical dynamical models, mass and momentum flux theory, and parametrization. *Quart. J. Roy. Meteor. Soc.*, **118**, 819–850, https://doi.org/10.1002/qj.49711850703.

Moncrieff, M. W., 2004: Analytic representation of the large-scale organization of tropical convection. *J. Atmos. Sci.*, **61**, 1521–1538, https://doi.org/10.1175/1520-0469(2004)061<1521:AROTLO>2.0.CO;2.

Moncrieff, M. W., Liu, C., & Bogenschutz, P. (2017). Simulation, modeling, and dynamically based parameterization of organized tropical convection for global climate models. Journal of the Atmospheric Sciences, 74, 1363–1380. https://doi.org/10.1175/JAS-D-16-0166.1

Nesbitt, S. W., Cifelli, R., & Rutledge, S. A. (2006). Storm morphology and rainfall characteristics of TRMM precipitation features. Monthly Weather Review, 134, 2702–2721. https://doi.org/10.1175/MWR3200.1

Prein, A.F., Liu, C., Ikeda, K. *et al*. Simulating North American mesoscale convective systems with a convection-permitting climate model. *Clim Dyn* **55,** 95–110 (2020). https://doi.org/10.1007/s00382-017-3993-2

Pandya, R. E., and D. R. Durran, 1996: The influence of convectively generated thermal forcing on the mesoscale circulation around squall lines. *J. Atmos. Sci.*,**53,** 2924–2951.

Parker, M. D., and R. H. Johnson (2000). Organizational modes of midlatitude mesoscale convective systems. *Mon. Wea. Rev.*, **128**, 3413–3436, https://doi.org/10.1175/1520-0493(2001)129<3413:OMOMMC>2.0.CO;2.

Parker, M. D., & Johnson, R. H. (2004). Structures and Dynamics of Quasi-2D Mesoscale Convective Systems, *Journal of the Atmospheric Sciences*, *61*(5), 545-567. Retrieved Feb 24, 2022, from https://journals.ametsoc.org/view/journals/atsc/61/5/1520-0469_2004_061_0545_sadoqm_2.0.co_2.xml

Rotunno, R., J. B. Klemp, and M. L. Weisman, 1988: A theory for strong, long-lived squall lines. J. Atmos. Sci., 45, 463–485, https://doi.org/10.1175/1520-0469(1988)045,0463:ATFSLL.2.0.CO;2.

Stevens, B., et al. (2020). The added value of large-eddy and storm-resolving models for simulating clouds and precipitation. *Journal of the Meteorological Society of Japan*, *98*, 395-435. doi:10.2151/jmsj.2020-021 [Fulltext]

Thorpe, A. J., M. J. Miller, and M. W. Moncrieff, 1982: Two-dimensional convection in a non-constant shear: A model of midlatitude squall lines. *Quart. J. Roy. Meteor. Soc.*, **108**, 739–762, https://doi.org/10.1002/qj.49710845802.

Weisman, M L., J B. Klemp, and R. Rotunno, 1988: Structure and evolution of numerically simulated squall lines. *J. Atmos. Sci.*, **45 ,** 1990–2013.

Weisman, M. L., and R. Rotunno, 2004: ‘‘A theory for strong, long-lived squall lines’’ revisted. J. Atmos. Sci., 61, 361–382.

Xie, S., Wang, Y.-C., Lin, W., Ma, H.-Y., Tang, Q., Tang, S., et al. Zhang, M (2019). Improved diurnal cycle of precipitation in E3SM with a revised convective triggering function. Journal of Advances in Modeling Earth Systems, 11, 2290– 2310. https://doi.org/10.1029/2019MS001702

Xu, Q., 1992: Density currents in shear flows—A two-fluid model. *J. Atmos. Sci.*,**49,** 511–524.

Xue, Ming, 2007, "Density currents in two-layer shear flows" Quarterly Journal of the Royal Meteorological Society Vol. 126, No. 565, pp 1301, 1477870X

Table and Figure Captions

Table 1. Governing equation, boundary conditions, and momentum budget in the three flows. The numbers in the parenthesis at the end of each equation are the equation numbers in the text.

Table 2. Governing equation, boundary conditions of the far-side solution in the three flows. The numbers in the parenthesis at the end of each equation are the equation numbers in the text.

Table 3. Constraints on the global properties. The numbers in the parenthesis at the end of each equation are the equation numbers in the text.

Figure 1. Conceptual model of the kinematic, microphysical, and radar echo structure of a squall line viewed in a vertical cross section oriented perpendicular to the convective line. Adapted from Figure 17.12 in Houze (2018).

Figure 2. Streamline (ψ) and the natural coordinate system with tangential and perpendicular forces F_s and F_n to accelerate the flow or bend the streamline.

Figure 3. Schematics of the solution domains and streamlines of the jump flow, the overturning circulation, and the backside flow. The blue streamlines separate the three flows. z_R is the altitude of the inflow separating the jump flow and the overturning circulation. z_S is the altitude separating the inflow and outflow in the overturning circulation. z_c is the altitude separating the jump flow and the backside flow on the far left. z_b is the altitude separating the inflow and outflow in the cold pool. The environmental wind profile is $U_0(z)$; the relative inflow is $u_0(z) = U_0(z) - c$, where c is the propagation speed of the squall line.

Figure 4. (a)-(c) Specified buoyancy (unit in 10^{-2} kg m/s^2), calculated CAPE (unit in 10 J), and a component of the vorticity source factor in the toy-model on the backside. The abscissa is the origination altitude of a parcel. The ordinate is the arrival altitude. The values of the x-axis is reversed. (d) The far-side flow speed (unit in m/s).

Figure B1. Circulation and horizontal vorticity in the x-z plane.

Table 1. Governing equation, boundary conditions, and momentum budget in the three flows. The numbers in the parenthesis at the end of each equation are the equation numbers in the text.

governing Equation	$\frac{\partial^2\psi}{\partial x^2}+\frac{\partial^2\psi}{\partial z^2}+\frac{1}{H_s}\frac{\partial\psi}{\partial z}=F(\psi,z)$ (40) $F(\psi,\mathrm{z})=\rho(z)^2\frac{\eta_0[z_0(\psi)]}{\rho[z_0(\psi)]}-\frac{1}{\rho[z_0(\psi)]\,u_0[z_0(\psi)]}G[z_0(\psi),\mathrm{z}]$ (41) $\frac{\partial\psi}{\partial z_0}=\rho(z_0)u_0(z_0)$ (19), $\eta_0=\frac{\partial u_0}{\partial z_0}$ (38), $G(z_0,z)=-\frac{\partial CAPE(z_0,z)}{\partial z_0}$ (32)		
flow	jump flow (ascending front-to-rear flow)	Overturning flow	backside or cold pool flow (descending rear inflow)
solution domain	$x\in[-L\ ,L]$ $z\geq h_0(x),\psi[x,h_0(x)]=0;$ $z\leq h_R(x),\psi[x,h_R(x)]=\psi_R$	$x\in[-L\ ,L]$ $z\geq h_R(x),\psi[x,h_R(x)]=\psi_R;$ $z\leq H$	$x\in[-L\ ,0]$ $z\geq 0$; $z\leq h_0(x),\psi[x,h_0(x)]=0$
upper boundary condition	$\psi[x,h_R(x)]=\psi_R$ (49); $\lvert\nabla\psi\rvert^2=\lvert\nabla\psi\rvert^2_{overturning\ flow}$ at $z=h_R(x)$ (97)	$\psi(x,H)=\psi_R$ (94)	$\psi[x,h_0(x)]=0$ (122); $-\frac{1}{2\rho}\lvert\nabla\psi\rvert^2+$ $\rho\left[\mathrm{CAPE_b}(z_c,z)+\frac{1}{2}u_{z_c}^2\right]=$ $\left\{-\frac{1}{2\rho}\lvert\nabla\psi\rvert^2+\right.$ $\rho\left[\mathrm{CAPE}(0,z)+\right.$ $\left.\left.\frac{1}{2}u_0^2(0)\right]\right\}_{jump\ flow}$ (124)
lower boundary condition	$\psi[x,h_0(x)]=0$ (48); $-\frac{1}{2\rho}\lvert\nabla\psi\rvert^2+\rho\left[\mathrm{CAPE}(0,z)+\right.$ $\left.\frac{1}{2}u_0^2(0)\right]=\left\{-\frac{1}{2\rho}\lvert\nabla\psi\rvert^2+\right.$ $\rho\left[\mathrm{CAPE_b}(z_c,z)+\right.$ $\left.\left.\frac{1}{2}u_{z_c}^2\right]\right\}_{backside\ flow}$ at $z=h_0(x)$ (124)	$\psi[x,h_R(x)]=\psi_R$ (95) $\lvert\nabla\psi\rvert^2=\lvert\nabla\psi\rvert^2_{jump\ flow}$ at $z=h_R(x)$ (97)	$\psi(x,0)=0$ (123)
boundary condition at $x=-L$	Far-side solution	N/A	Far side solution
boundary condition at $x=L$	$\psi(x=L,z)=\psi_R+$ $\int_0^z\rho_0u_0\,dz$ for $z\in[0,z_R]$ (43)	$\psi(x=L,z)=\psi_R+$ $\int_{z_R}^z\rho_0u_0\,dz$ for $z\in[z_R,z_s]$ (98); Far side solution for $z\in[z_s,H]$	N/A
Momentum budget	$\left[\int_{z_c}^H\rho u^2\,dz+\right.$ $\left.\int_{z_c}^H p dz\right]_{x=-L\ in\ jump\ flow}=$ $\left[\int_0^{z_R}\rho u_0^2dz_0\right]_{x=L\ in\ jump\ flow}+$ $(P_{\psi=\psi_R}-P_{\psi=0})$ (56)	$P_{\psi=\psi_R}=\left[\int_{z_R}^{z_s}\rho u_0^2dz+\right.$ $\int_{z_s}^H\rho u^2dz+$ $\left.\int_{z_s}^H p\,dz\right]_{x=L\ in\ overturning\ flow}$ (105)	$P_{\psi=0}=\left[\int_0^{z_b}u^2dz+\right.$ $\int_{z_b}^{z_c}u_0^2dz+$ $\left.\int_0^{z_c}pdz\right]_{x=-L\ in\ backside\ flow}$ (140)

Table 2. Governing equation, boundary conditions of the far-side solution in the three flows. The numbers in the parenthesis at the end of each equation are the equation numbers in the text.

governing Equation	$\frac{d^2\psi}{dz^2}+\frac{1}{H_s}\frac{d\psi}{dz}= F(\psi,z)$ (44) $F(\psi,\mathrm{z})=\rho(z)^2\frac{\eta_0[z_0(\psi)]}{\rho[z_0(\psi)]}-\frac{1}{\rho[z_0(\psi)]\,u_0[z_0(\psi)]}G[z_0(\psi),\mathrm{z}]$ (41) $\frac{\partial\psi}{\partial z_0}=\rho(z_0)u_0(z_0)$ (19), $\eta_0=\frac{\partial u_0}{\partial z_0}$ (38), $G(z_0,z)=-\frac{\partial CAPE(z_0,z)}{\partial z_0}$ (32)		
flow	jump flow (ascending front-to-rear flow)	overturning flow	backside or cold pool flow (descending rear inflow)
solution domain	outflow $x=-L, z\,\epsilon\,[z_c,H]$	outflow $x=L, z\,\epsilon\,[z_s,H]$	outflow $x=-L, z\,\epsilon\,[0,z_b]$ inflow $x=-L, z\,\epsilon\,[z_b,z_c]$
upper boundary condition	$\psi(H)=\psi_R$ (49)	$\psi(z_s)=\psi_s$ (94)	$\psi(z_c)=0$ (122)
lower boundary condition	$\psi(z_c)=0$ (48)	$\psi(H)=\psi_R$ (95)	$\psi(0)=0$ (123)
toy model	Section 3.4	Section 4.4	Section 5.3

Table 3. Constraints on the global properties. The numbers in the parenthesis at the end of each equation are the equation numbers in the text.

global properties	c propagation speed z_c cold pool height z_R depth of the jump flow z_s steering-level height z_b separation height of the backside inflow and outflow	ψ_R mass flux of the jump flow ψ_s total mass flux of the jump flow and overturning circulation ψ_B mass flux of the backside flow u_{b0} backside surface flow speed $P_{\psi=0}$ horizontal pressure force between cold pool and jump flow $P_{\psi=\psi_R}$ horizontal pressure force between overturning and jump flows
constraint on propagation speed c	$(1-\frac{\rho_0}{\rho_{z_c}})u_{00}^2 = u_{b0}^2 - u_{z_c}^2 - 2\int_0^{z_c} B_c(z)\mathrm{dz}$ (151)	
constraint on cold pool height z_c	$\left[\int_0^{z_b} u^2 dz + \int_{z_b}^{z_c} u_0^2 dz + \int_0^{z_c} p dz\right]_{\substack{x=-L\ in \\ backside\ flow}} + \left[\int_{z_c}^{H} \rho u^2\, dz + \int_{z_c}^{H} p dz\right]_{\substack{x=-L\ in \\ jump\ flow}}$ $= \left[\int_0^{z_R} \rho u_0^2 dz_0\right]_{\substack{x=L\ in \\ jump\ flow}} + \left[\int_{z_R}^{z_s} \rho u_0^2 dz + \int_{z_s}^{H} \rho u^2 dz + \int_{z_s}^{H} p\, dz\right]_{\substack{x=L\ in \\ overturning\ flow}}$ (156)	
constraint on jump flow depth z_R	$\int_{z_R}^{z_s} \rho u_0(z_0) dz_0 + \int_{z_s}^{H} \rho u dz = 0$ (103)	
steering level z_s	$U(z_s) = c$ (100)	
constraint on separation height of the backside inflow and outflow z_b	$\begin{pmatrix} u \\ z_0 \end{pmatrix}\Big\|_{z=z_b} = \begin{pmatrix} 0 \\ z_b \end{pmatrix}$ (136)	
mass flux of the jump flow ψ_R	$\psi_R = \int_0^{z_R} \rho u_0(z_0)\, dz_0$ (42)	
total mass flux of the jump flow and overturning circulation ψ_s	$\psi_s = \psi_R + \int_{z_R}^{z_s} \rho u_0\, dz$ (98)	
mass flux of the backside flow ψ_B	$\psi_B = \int_{z_b}^{z_c} \rho u\, dz$ (38)	
backside surface flow speed u_{b0}	$\begin{pmatrix} u \\ z_0 \end{pmatrix}\Big\|_{z=z_b} = \begin{pmatrix} 0 \\ z_b \end{pmatrix}$ (136)	
horizontal pressure force between cold pool and jump flow $P_{\psi=0}$	$P_{\psi=0} = \left[\int_0^{z_b} u^2 dz + \int_{z_b}^{z_c} u_0^2 dz + \int_0^{z_c} p dz\right]_{\substack{x=-L\ in \\ backside\ flow}}$ (140)	
horizontal pressure force between overturning and jump flows $P_{\psi=\psi_R}$	$P_{\psi=\psi_R} = \left[\int_{z_R}^{z_s} \rho u_0^2 dz + \int_{z_s}^{H} \rho u^2 dz + \int_{z_s}^{H} p\, dz\right]_{\substack{x=L\ in \\ overturning\ flow}}$ (105)	

Figures

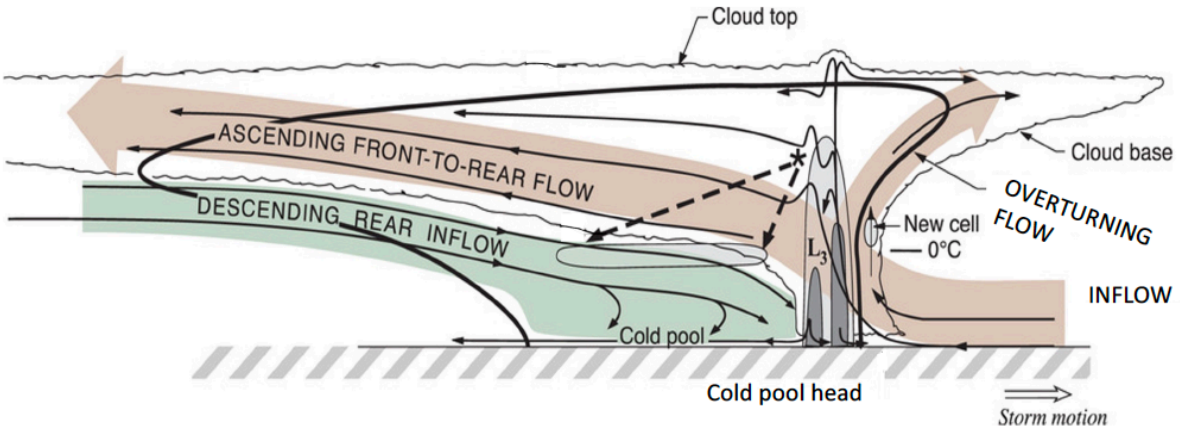

Figure 1. Conceptual model of the kinematic, microphysical, and radar echo structure of a squall line viewed in a vertical cross section oriented perpendicular to the convective line. Adapted from Figure 17.12 in Houze (2018).

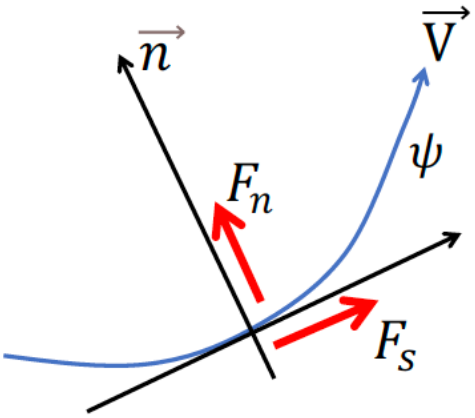

Figure 2. Streamline (ψ) and the natural coordinate system with tangential and perpendicular forces F_s and F_n to accelerate the flow or bend the streamline.

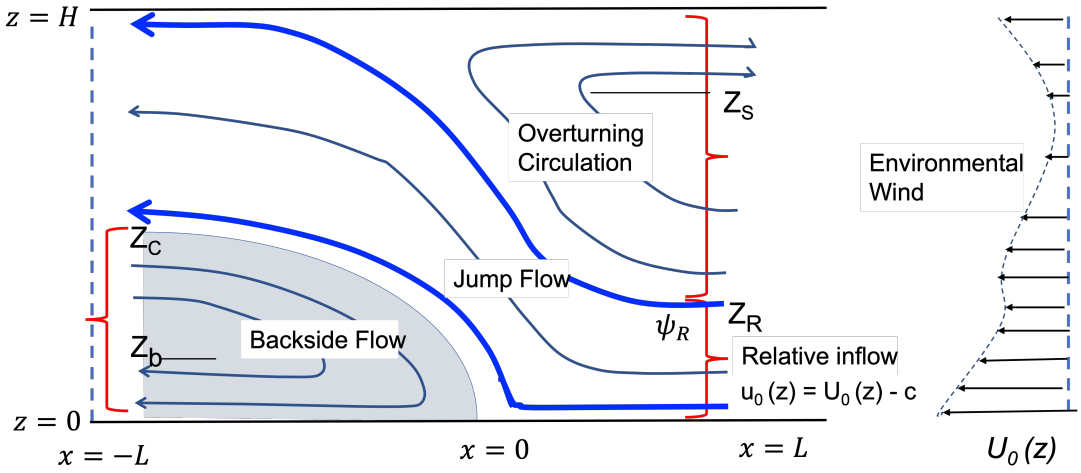

Figure 3. Schematics of the solution domains and streamlines of the jump flow, the overturning circulation, and the backside flow. The blue streamlines separate the three flows. z_R is the altitude of the inflow separating the jump flow and the overturning circulation. z_S is the altitude separating the inflow and outflow in the overturning circulation. z_c is the altitude separating the jump flow and the backside flow on the far left. z_b is the altitude separating the inflow and outflow in the cold pool. The environmental wind profile is $U_0(z)$; the relative inflow is $u_0(z) = U_0(z) - c$, where c is the propagation speed of the squall line.

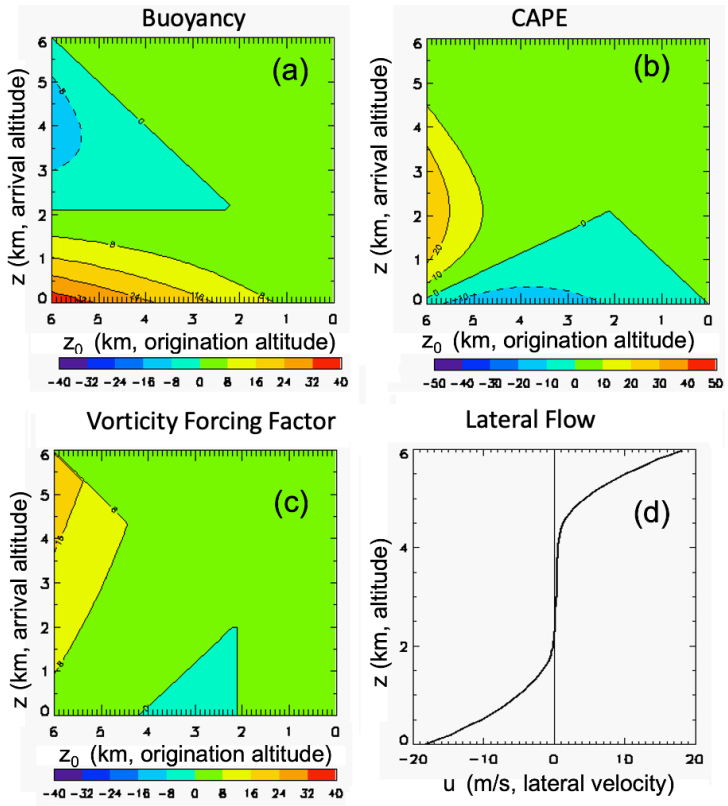

Figure 4. (a)-(c) Specified buoyancy (unit in 10^{-2} kg m/s^2), calculated CAPE (unit in 10 J), and a component of the vorticity source factor in the toy-model on the backside. The abscissa is the origination altitude of a parcel. The ordinate is the arrival altitude. The values of the x-axis is reversed. (d) The far-side flow speed (unit in m/s).

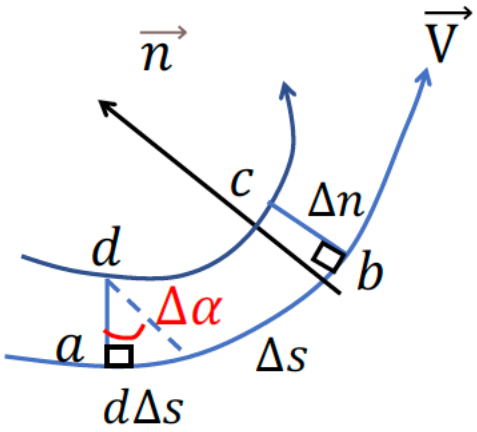

Figure B1. Circulation and horizontal vorticity in the x-z plane.